Mohamed Khider University of Biskra
Faculty of exact sciences and natural and life sciences
Material sciences department

MASTER MEMORY

Matter sciences
Physics
Material physics

Ref. :

Prsented by:
Hanane Mebarki
10/06/2024

Study of $CH_3NH_3PbI_3$ perovskite-based solar cells performance

---

Jury:

Mme	Bariza BOUDOUR	MCB	University of Biskra	President
Mme	widad LAIADI	MCA	University of Biskra	Supervisor
Mme	Leila BOUDHIB	MAA	University of Biskra	Examiner

AcademicYear: 2023/2024

Table of contents

Table of contents

Dedication

In the name of Allah, the most gracious the most merciful, all praise to Him without him this work would never been done.

This work is dedicated to:

First of all to my great parents who supported me throughout my life and provided me with their love,

My cherished sisters "Nesrine" "Samia" "Achouak" " Selma ", who have never left my side and always inspire and push me to be a better person in this world.

and brothers " Badereddine " " Nasereddine " " Abdessalem " "Abderrahmane "

To my beloved little girl " Asma "

Family descendants " Souhaib " " Rahile " " Rahma " " Mohamed"

To my dear aunt

To my beloved second mother

To all who have passed by my life, left a beautiful mark in it, and have been a source of inspiration.

Thanks, and much appreciation to you all.

Aknowledgemets

In the Name of Allah, the Beneficent, the Merciful

Foremost, I am very grateful to Almighty Allah for without Him graces and blessing, this study would not have been possible. I thank him for giving me the strength and ability to complete this research.

I submit my heartiest gratitude to my respected Prof. Mme. Widad LAIADI for her sincere guidance and help for completing this work.

I extend my thanks to all concerned persons who co-operated with me in this regard and everyone who supported me and helped me to get my thesis

In addition to our consultant, I would like to thank jury members, M^{me} Bariza BOUDOUR, as president and M^{me}. Leila BOUDHIB as examiner

Abstract

The promising technology of $CH_3NH_3PbI_3$ perovskite solar cells is particularly interested in increasing efficiency. Solar cells based on perovskite represent an innovative approach to achieve the best possible photovoltaic performances. The main objective of this work is to study the performance of $CH_3NH_3PbI_3$ perovskite-based solar cells, using the SILVACO software. In this work, we examined the electrical characteristics (I-V) of the primary modelled solar cell, and The electrical outputs of the primary PSC solar cell obtained are the short-circuit current density Jsc, the open-circuit voltage Voc, the fill factor FF and the conversion efficiency η are 21.33 mA/cm2, 0.88 V, 0.72 and 14.44 %, respectively, agree with experimental data. On the other hand, the simulation enabled us to study the effect of the ETM region thickness, the effect of HTM region thickness and the last effect which is the replacing of the HTM region (Spiro-OMeTAD) with PEDOT: PSS on the electrical characteristics of the perovskite solar cell. Through the obtained results we noticed that the PEDOT: PSS material improved the characteristics (I-V) of the perovskite solar cell and the optimum parameters of the thickness of ETL and HTL layers which are 0.1 µm, in the two cases. the obtained output parameters of the solar cell improved in the case of the optimum thickness of ETL are Jsc= 27.91 mA/cm2, Voc= 0.88 V, FF= 0.72 and η= 17.71% While in the case of the optimum thickness of HTL are Jsc= 27.2 mA/cm2, Voc= 0.88 V, FF= 0.72 and η= 17.61%.

الملخص

تهتم التكنولوجيا الواعدة للخلايا الشمسية البيروفسكايت $CH_3NH_3PbI_3$ بشكل خاص بزيادة الكفاءة. تمثل الخلايا الشمسية المعتمدة على البيروفسكايت نهجًا مبتكرًا لتحقيق أفضل أداء ممكن للطاقة الكهروضوئية. الهدف الرئيسي من هذا العمل هو دراسة أداء الخلايا الشمسية المعتمدة على البيروفسكايت $CH_3NH_3PbI_3$ ، باستخدام برنامج SILVACO. في هذا العمل، قمنا بفحص الخصائص الكهربائية (I-V) للخلية الشمسية النموذجية الأولية، والمخرجات الكهربائية للخلية الشمسية PSC الأولية التي تم الحصول عليها هي كثافة تيار الدائرة القصيرة Jsc، جهد الدائرة المفتوحة Voc، عامل التعبئة FF وكفاءة التحويل η هي 21.33 مللي أمبير/سم2، 0.88 V، 0.72 و14.44%، على التوالي،والتي تتفق مع البيانات التجريبية. من ناحية أخرى مكنتنا المحاكاة من دراسة تأثير سمك منطقة ETM وتأثير سمك منطقة HTM والتأثير الأخير وهو استبدال منطقة HTM (Spiro-OMeTAD) بـ PEDOT: PSS على الخصائص الكهربائية لخلية البيروفسكايت الشمسية. من خلال النتائج التي تم الحصول عليها لاحظنا أن مادة PEDOT: PSS حسنت خصائص (I-V) للخلية الشمسية البيروفسكايت والمعلمات المثلى لسمك طبقات ETL و HTL والتي تبلغ 0.1 ميكرومتر في الحالتين. معلمات الخرج التي تم الحصول عليها للخلية الشمسية المحسنة في حالة السُمك الأمثل لـ ETL هي Jsc = 27.91 مللي أمبير / سم 2، Voc = 0.88 V، FF = 0.72 و ٪17.71 = η بينما في حالة السُمك الأمثل لـ HTL هي Jsc= 27.2 مللي أمبير/سم2، Voc= 0.88V ، FF= 0.72 و 17.61% =η.

List of figures

List of figures

List of tables

List of abbreviations

PV: Photovoltaic.

λ : Wavelength.

Eg: Gap energy

Nc: Effective density of conduction band

Nv: Effective density of valence band

μ_n: Electron mobility

μ_p: Hole mobility

ε_r : Relative dielectric constant

HOMO: Highest occupied molecular orbital

LUMO: Lowest unoccupied molecular orbital

J-V: Current –density vs .voltage

Jsc: short circuit current

Voc: Open circuit voltage

FF: Fill factor

PCE: Power conversion efficiency

PSCs: Perovskite solar cell

ETL: Electron transport layer

HTL: Hole transport layer

ETM: Electron transport material

FTO: Fluorine-doped tin oxide

TiO_2: Titanium dioxide

$CH_3NH_3I_3$: Organic components

VASP: Vacuum-assisted solution process

MAPbI3: Methylamo,ium lead iodide

Silvaco: Silicon valley comporation

DDSS: Dye-sensitized solar cells

I: Iodide

Pb: Lead

OPV: Organic photovoltaic.

Introduction

Introduction

"Semiconductor Devices save the Earth." This unusually title of a scientific research called attention to the potential of solar cells as one solution to the global energy and climate warming problems. Suppose the rate of world consumption of energy does not grow with time but stays at its present level. The confirmed global oil reserve will last about 35 years. It is 60 years for natural gas, 170 years for coal, and 60 years for uranium. If our consumption rate increases by only 3% a year, the projected energy consumption will deplete the fossil fuel reserves even sooner. Although new reserves may be discovered from time to time, there is the additional problem of global warming (greenhouse effect) caused by the emission of carbon dioxide from burning fossil fuels [1]. It would be foolhardy not to aggressively conserve energy and develop renewable energy sources such as solar cells. Solar energy can be converted into electricity through many means besides photovoltaics. For example, it is converted into heat that drives a thermal engine that drives an electric generator in a solar thermal-electric system. Wind electricity generation harnesses the energy of the wind, which is created by solar heating of the earth. Growing plants and then burning them to generate electricity is another way. They all generate electricity without net emission of carbon dioxide [2].

Due to the increasing demand for clean energy, much research effort has been dedicated to the improvement of solar energy technologies. As a result, in 2013 Grätzel's group created a mesoporous hybrid organic-inorganic perovskite solar cell (PSC) with certified power conversion efficiency (PCE) of 15 % [1]. At the same time, Snaith's group also succeeded in creating a planar organic-inorganic perovskite solar cell with PCE of 15.4 % [2]. In the prominent scientific journal "Nature", these PSCs were described as one of the ten greatest scientific achievements of 2013 [3]. Since the time of these achievements, the research into PSCs has grown rapidly, which has been described as a "perovskite fever" [4], and in 2019 the efficiency of the PSCs reached 24.2 % [5]. These astonishing efficiencies are attributed to the very interesting electronic and optical properties of the perovskite layer [6], [7]. The most studied compound for the perovskite solar cells is methyl ammonium lead triiodide ($CH_3NH_3PbI_3$). It has a charge carrier mobility of 8 cm^2 / (V·s) in thin polycrystalline layers [6], but this

quantity is much higher for monocrystals, reaching 105±35 cm^2 /(V·s) [7]. These perovskites also have extremely low charge carrier recombination rates for both the monomolecular and the bimolecular recombinations [6]. In addition, they feature an ambipolar charge transport with a balanced electron and hole diffusion lengths, these being greater than 100 nanometers in a polycrystalline CH_3NH_3 PbI_3 layer [8], [9]. In monocrystals, though, the electron and the hole diffusion lengths exceed 175 μm under illumination of nominal full sunlight intensity and even 3 mm under 1000 times weaker illumination [7]. The aforementioned features of trihalide perovskites provide long lifetime of photogenerated charge carriers [6], [7], [9]. These perovskites have a broad absorption spectrum covering all the visible range up to 800 nm on the red side, with a high absorption coefficient from $5 \cdot 10^4$ up to $5 \cdot 10^5$ cm^{-1}. Commonly, a thickness of 300 - 400 nm is sufficient for such a perovskite to fully absorb the incident visible light [8], [9].

This work presents a Study of $CH_3NH_3PbI_3$ perovskite-based solar cells performance, the first chapter gives a general concept of Solar Cells, And solar cells' characteristics. Chapter II focused on perovskite solar cell material and its properties and Photovoltaic problems that hinder their efficiency and stability have been the subject of extensive research in recent years. Researchers have focused on developing hole transport layers and electron transport layers using various materials. Chapter III summarizes the simulation software and the main parameters used. And discusses the results obtained in this work.

Chapter I:
General Concepts of Solar Cells

I.1 Introduction

Solar cells are typically named after the semiconducting material they are made of. These materials must have certain properties in order to absorb sunlight. Some cells are designed to process sunlight reaching the Earth's surface, while others are optimized for use in space [10]. Solar cells can consist of just a single layer of light-absorbing material (single junction) or they can use multiple physical configurations (multijunction) to take advantage of different absorption and charge separation mechanisms.

I.2 Absorption of light

When light falls onto semiconductor material, photons with energy (Eph) less than the bandgap energy (Eg) interact only weakly with the semiconductor, passing through it as if it were transparent. However, photons with energy greater than the bandgap energy (Eph > Eg) interact with electrons in covalent bonds, using up their energy to break bonds and create electron-hole pairs, which can then wander off independently [10]. This is illustrated in Fig. I.1.

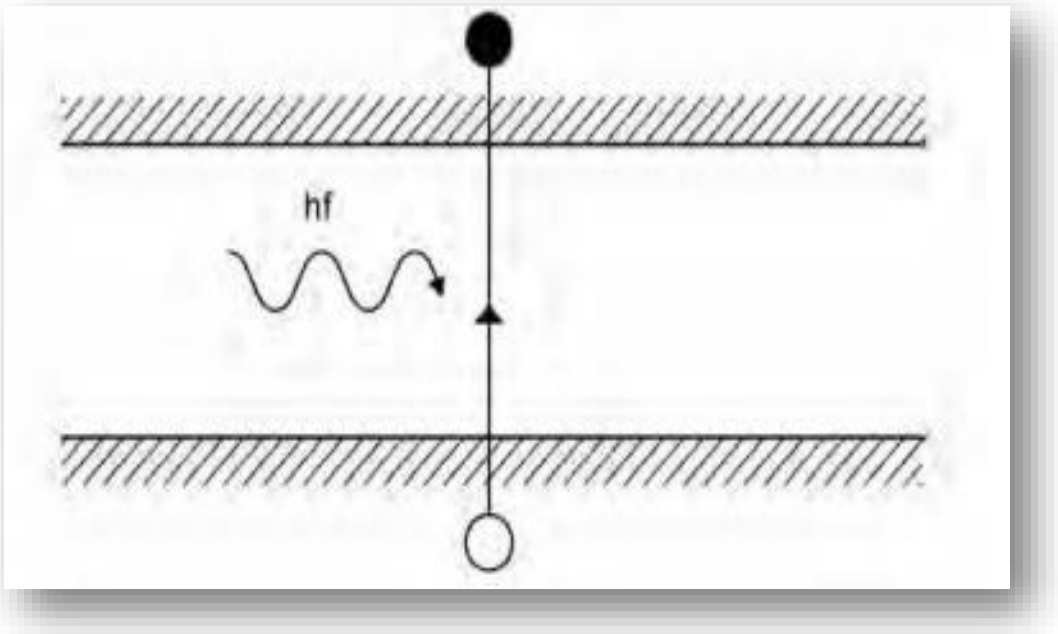

Figure I.1: The creation of electron-hole pairs when illuminated with light of energy.

Higher energy photons are absorbed closer to the surface of the semiconductor than lower energy photons, as illustrated in Fig. I.2.

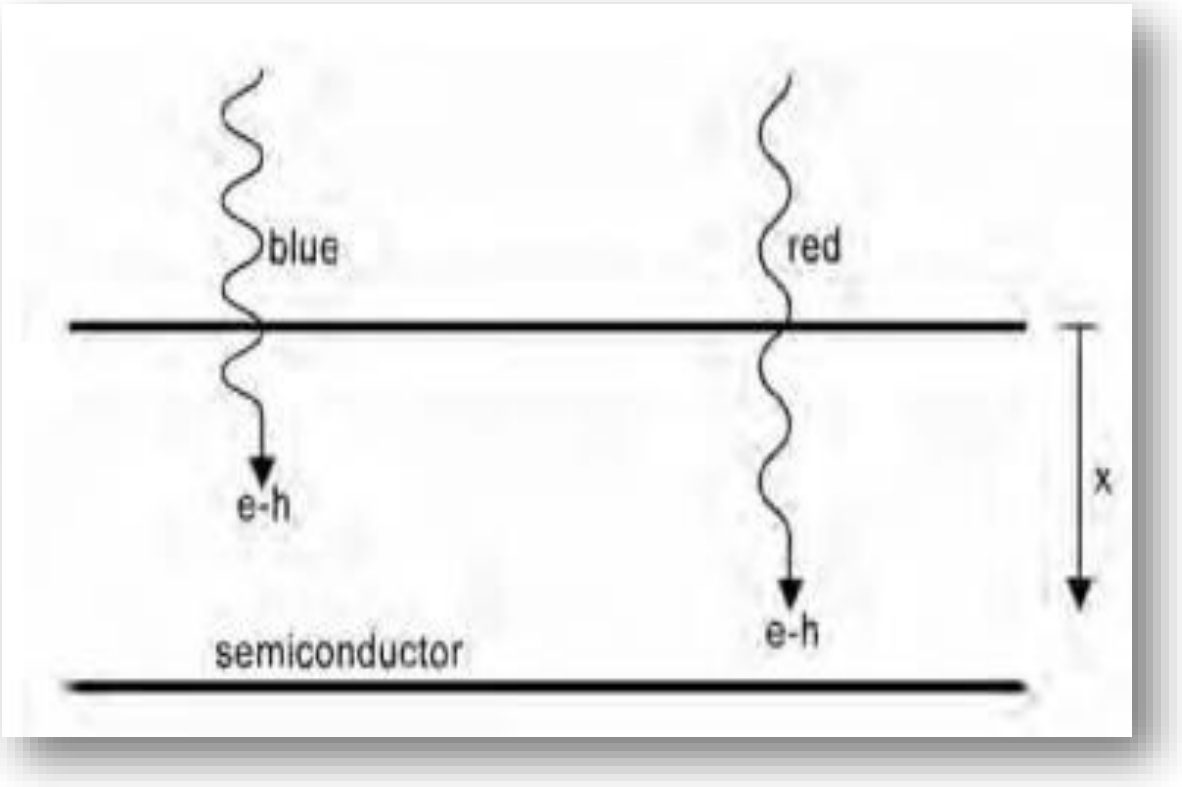

Figure I.2: The light energy dependency of electron-hole generation.

The generation rate (G) of electron-hole (e-h) pairs per unit volume can be calculated using the formula:

$$G = \alpha N e^{-\alpha x} \qquad \text{(I.1)}$$

Where N is the photon flux (photons per unit area per second), α is the absorption coefficient, and x is the distance from the surface. The value of α as a function of the wavelength of light is illustrated in Fig. I.3 for silicon at 300 K.

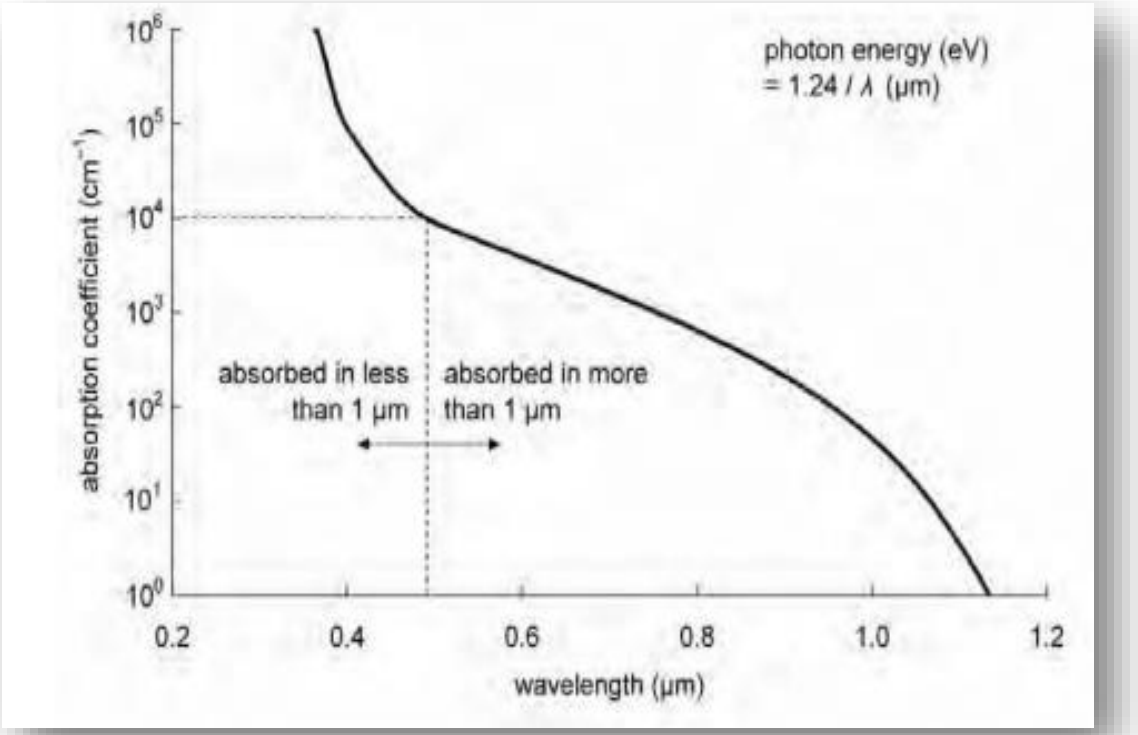

Figure I.3: The absorption coefficient of silicon at 300 K as a function of the vacuum wavelength of light.

I.3 The solar spectrum

The radiation from the sun may be modeled by that of a black body at a temperature of about 6000 K. Measurements of the solar radiation are made at the earth (not at the surface of the sun) so are lower intensity than that given by the Planck spectrum by the ratio (Rs/r_{es}), where Rs is the sun's radius and r_{se} is the mean distance between the earth and sun. Moreover, the sun's radiation has to pass through the earth's atmosphere before reaching the surface which slightly reduces its intensity [11]. The spectrum is plotted in the figure below reduced by the appropriate geometric factor. The blue curve is the theoretical spectrum and the green curve is the actual measured spectrum. Note that absorption in the atmosphere removes certain wavelengths nearly entirely [12].

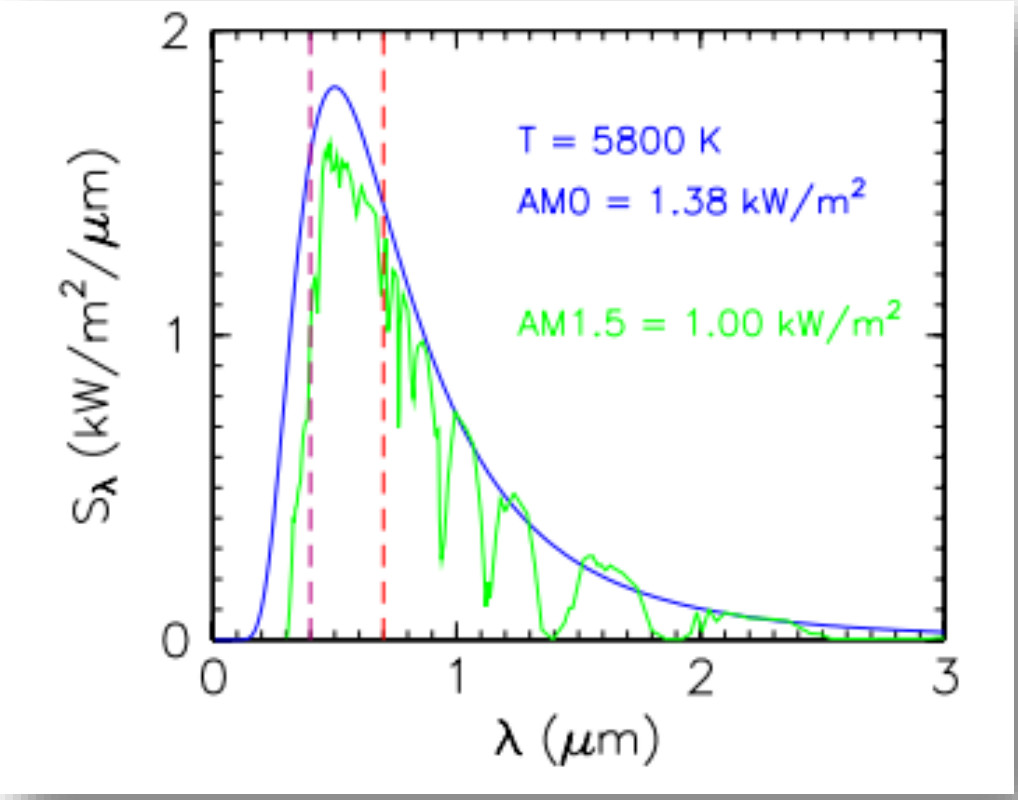

Figure I.4: The blue curve (smooth) is calculated from the above formula for a temperature T = 6000 K. The green curve (jagged) is the measured solar spectrum. Both curves are adjusted for distance from the sun. The dashed vertical lines indicate the visible spectrum, 400 nm - 700 nm.

I.4 Semiconductors

Semiconductor is a substance with a certain degree of conductivity between a conductor and an insulator. Physical conductivity is tied to its resistance to current flow. In other words, the higher the conductivity level and the lower is the resistance [10]. Fig.I.5 illustrates the electrical conductivityσ of certain materials from the three parts (and the corresponding resistivity $\rho = 1/\sigma$). Insulators have very low conductivity and high resistivity in the range of 10^{-18}–10^{-8} S/cm such as a diamond (pure), fused quartz, and sulfur; and conductors have low resistivity and high conductivity such as copper and platinum, typically between 10^4 and 10^6 S/cm. Semiconductor's conductivities occur between insulators and conductors [13]. The temperature,

illumination, magnetic field, and minute amounts of impurity atoms affect a semiconductor's conductivity, the semiconductor becomes one of the important materials in conductivity for that purpose [1].

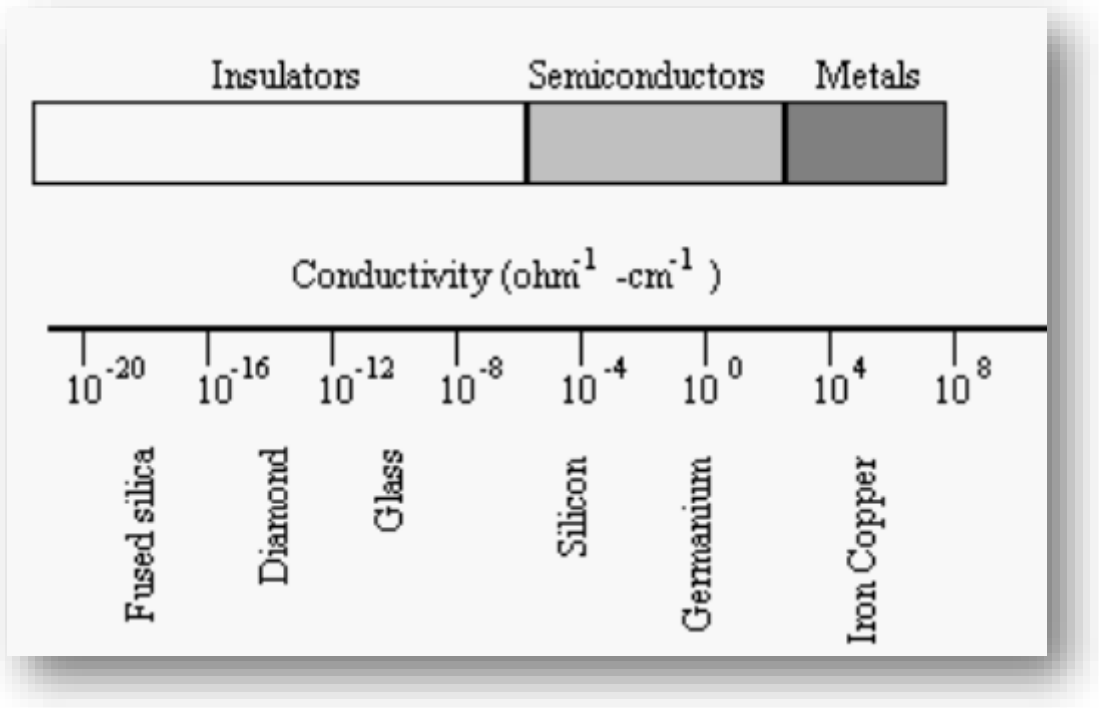

Figure I.5: Electrical conductivity at room temperature of some solid bodies; boundaries between semiconductors, metals and insulators.

I.5 Different types of doping

Intrinsic semiconductors are of little use. In fact, the semiconductor materials' properties can be substantially altered by adding impurity atoms to the proportionally pure semiconductor content. Though added, these impurities will reasonably alter the band structure to fully transform the material's electrical properties [2]. There are two types of semiconductors: N-doped semiconductors and P-doped semiconductors.

I.5.1 N-doped semiconductors

N-type doping is about amplifying the semiconductor electron density. Thus, the acceptor concentration will be lower than the donor concentration ($N_A < N_D$). For this, we include several

rich atoms in electrons in the semiconductor.

I.5.2 P-doped semiconductors

P-type doping is designed to increase the density of holes in the semiconductor, the concentration of acceptors would be higher than that of donors ($N_A > N_D$). For this reason, we include several poor atoms in electrons in the semiconductor [2].

I.6 PN Junction

A p-n junction is formed by joining n-type and p-type semiconductor materials, as shown in Fig. I.6.

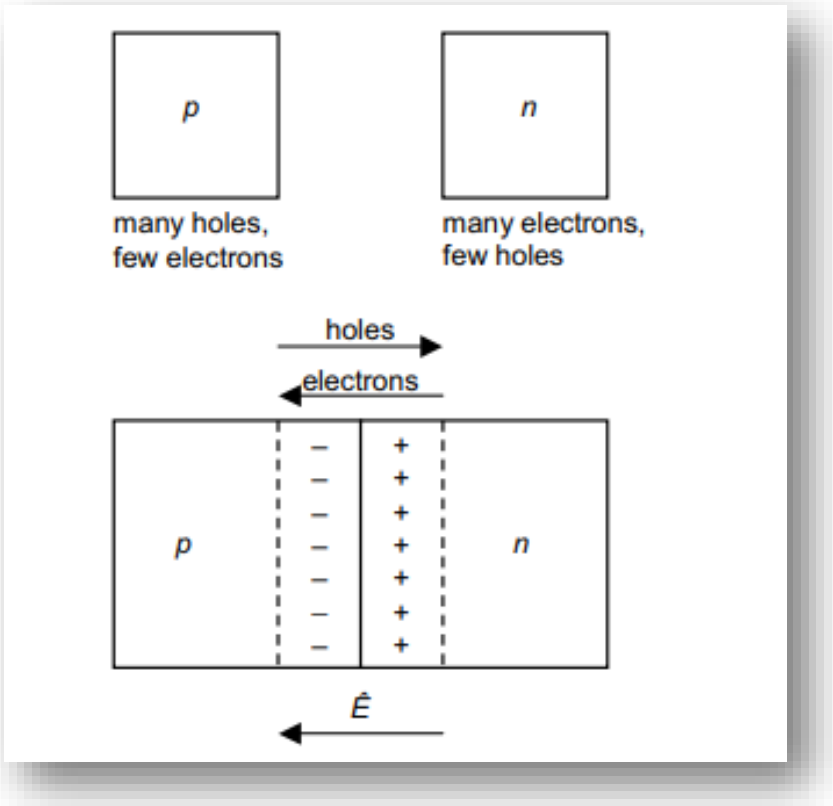

Figure I.6: Formation of a p-n junction.

When joined, the excess holes in the p-type material flow by diffusion to the n-type material, while electrons flow by diffusion from the n-type material to the p-type material as a result of

the carrier concentration gradients across the junction. The electrons and holes leave behind exposed charges on dopant atom sites, fixed in the crystal lattice. An electric field $\vec{E}$ therefore builds up in the so-called depletion region around the junction to stop the flow [14]. Depending on the materials used, a 'builtin' potential (Vbi) owing to $\vec{E}$ will be formed. If a voltage is applied to the junction, as shown in Fig. I.7, $\vec{E}$ will be reduced.

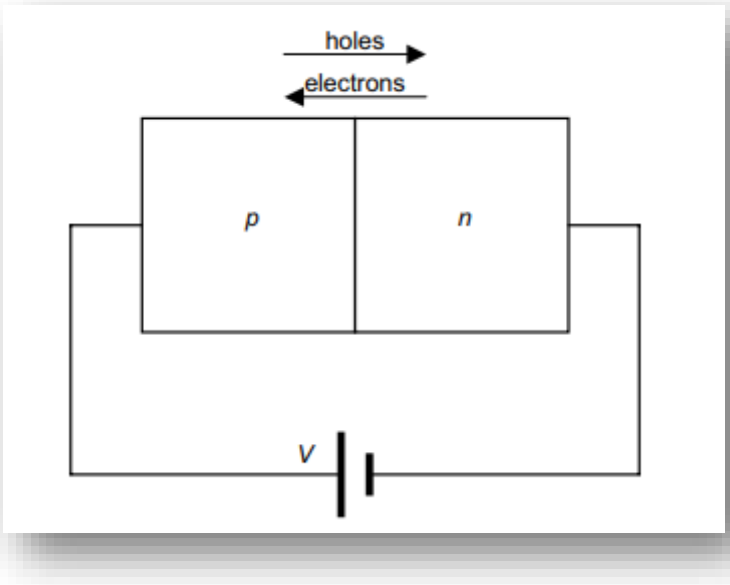

Figure I.7: Application of a voltage to a p-n junction.

Once $\vec{E}$ is no longer large enough to stop the flow of electrons and holes, a current is produced. The built in potential reduces to Vbi – V and the current flow increases exponentially with the applied voltage [14].

As illustrated in Fig. I.8, a PN junction can be fabricated by implanting or diffusing donors into a P-type substrate such that a layer of semiconductor is converted into N type. Converting a layer of an N-type semiconductor into P type with acceptors would also create a PN junction. A PN junction has rectifying current–voltage (I–V or IV) characteristics as shown in Fig. I.9. As a device, it is called a rectifier or a diode [15]. The PN junction is the basic structure of solar cell, light-emitting diode, and diode laser, and is present in all types of transistors. In addition,

PN junction is a vehicle for studying the theory of the depletion layer, the quasi-equilibrium boundary condition, the continuity equation, and other tools and concepts that are important to the understanding of PN junction.

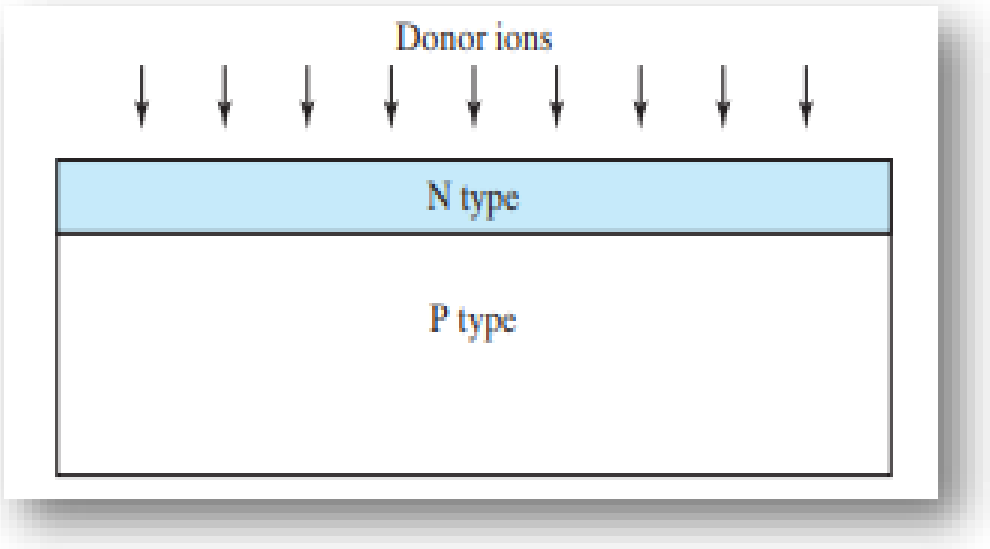

Figure I.8: PN junction can be fabricated by converting a layer of P-type semiconductor into N-type with donor implantation or diffusion.

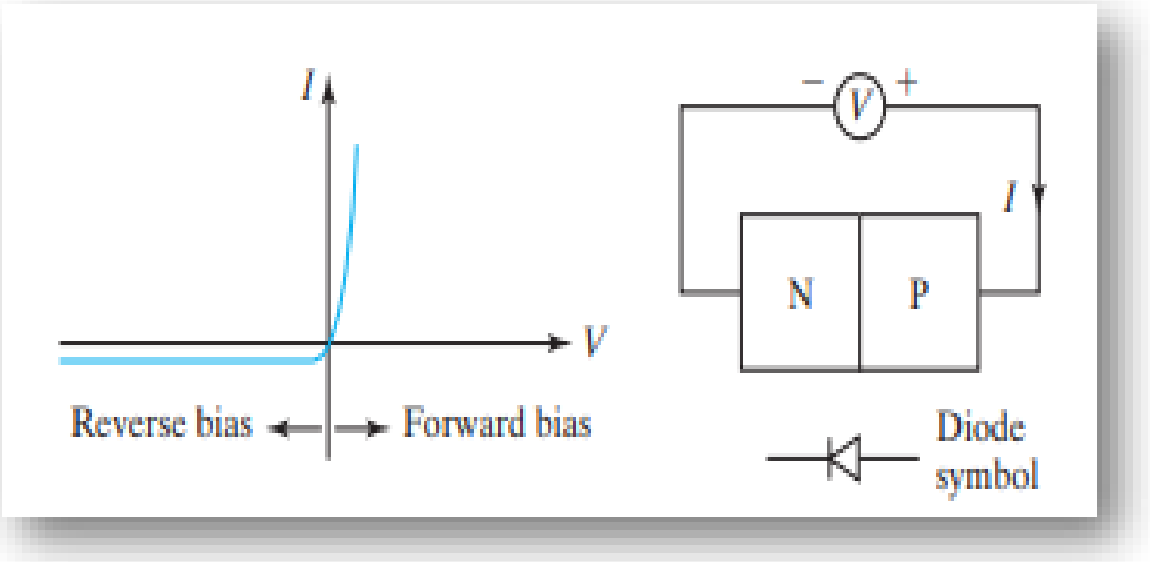

Figure I.9: The rectifying IV characteristics of a PN junction.

I.7 Solar cell

Solar cells are semiconductors that convert sunlight into direct current electricity (DC). Humans have a long history of utilizing solar energy for heat, but producing electricity is much more recent. It is closely linked to modern solid- state physics. A solar cell performs the photovoltaic influence; "photo" – light; "voltaic" – electricity (Fig I.10). In the PV effect, photons hit the surface of a semiconductor material such as silicon and release electrons from the material's atoms. Adding chemical compounds to the material's composition is very helpful for releasing electrons. This generates an electrical current. Over the photovoltaic influence, a typical 4-inch silicon solar cell can produce about a watt of DC electricity. Groups of photovoltaic cells can be electrically ordered into arrays and modules, which could be utilized to fresh batteries, motors, and supply energy of any number of electrical appliances [18]. Thin-film (PV) materials promise to decrease material requirements and manufacturing costs for photovoltaic modules and systems. Photovoltaic systems have unrivalled advantages over common power-generating technologies. PV systems could be designed for different sets of applications and operational needs and can be utilized for distributed power generation. It include no moving parts, are modular, easy to expand and even able to be carried in some cases. The features of photovoltaic systems are energy independence and environmental protection, which are both important. Firstly, sunlight is accessible and friendly to the environment, with no noise and pollution. Generally, if a photovoltaic system is designed well, it requires maintenance, which extends its long service life. Nowadays, the primary factor in constructing a PV system is the cost of photovoltaic modules and equipment compared to other energy sources [19].

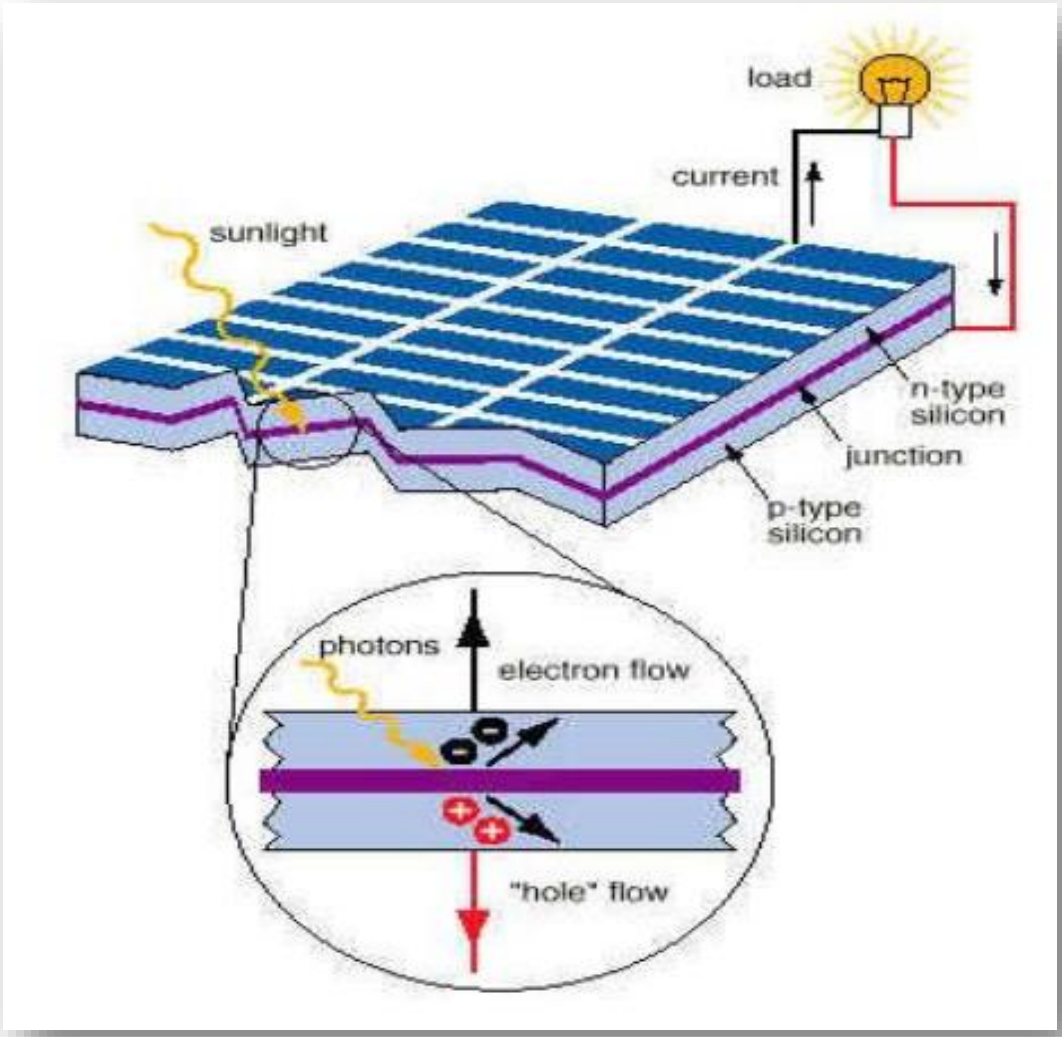

Figure I.10: Schematic of a typical solar cell.

I.8 Characteristic parameters of a photovoltaic cell

A solar cell is most often a p-n (or n-p) junction to which contacts are added to collect the current [19]. Once the solar cell is exposed to light, pairs of electron- hole are formed and thus the photogenerated I_{ph} current is created which depends on the amount of incident light. Fig.I.11 shows the solar cell's two I-V characteristics in the dark and under the illumination.

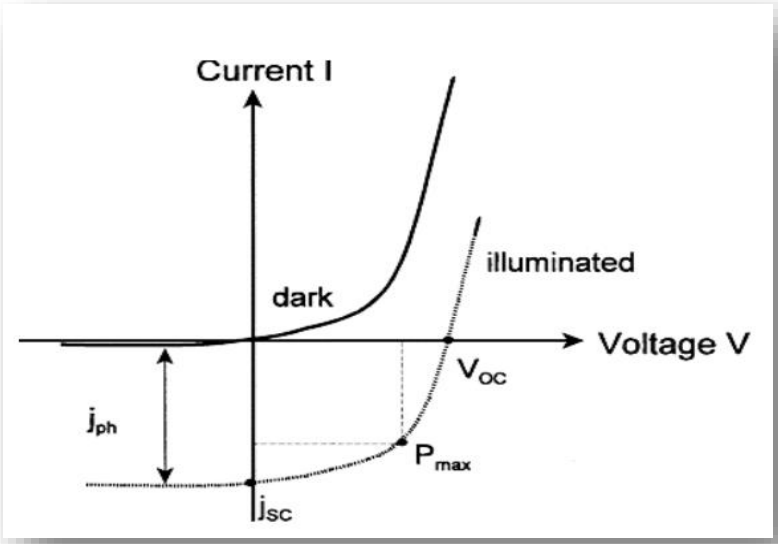

Figure I.11: I-V characteristics of the PV cell and its equivalent electric circuit.

I.8.1 Short circuit current Isc

It is noticed that the curve under illumination is displaced concerning the first value of Isc which explains the constant generation of current by light. This value is known as the short-circuit current, or it is the current that generates the cell under zero voltage under light.

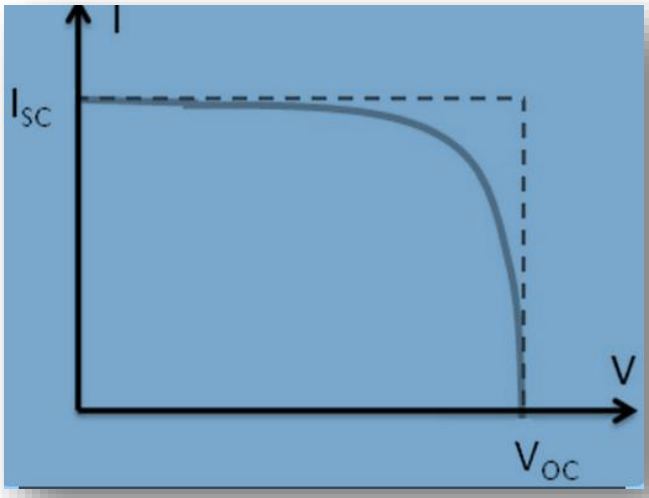

Figure I.12: Short circuit current Isc.

I.8.2 Open circuit voltage in V_{oc}

This is the open-circuit voltage, the voltage of the cell under zero current. In the ideal case, the short circuit current I_{sc} is equal to the photogenerated current I_{ph}.

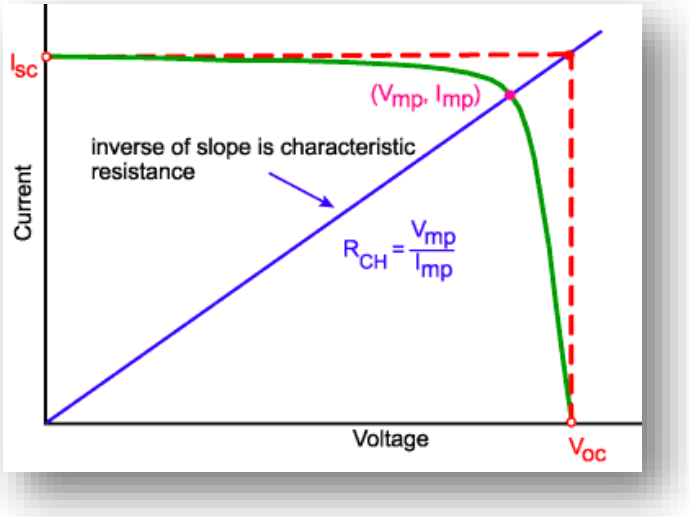

Figure I.13: open-circuit voltage.

I.8.3 Fill factor FF

The fill (form) factor indicates the cell quality that it develops the maximum power P_{max} at a voltage V_m and a current I_m, and it is handy to define the fill factor FF.

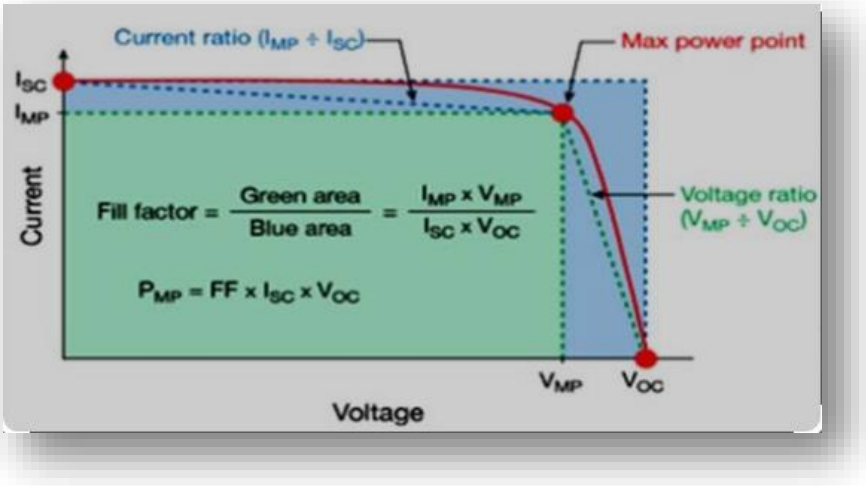

Figure I.14: Fill factor FF.

I.8.4 Energy conversion efficiency η

The energy efficiency or the conversion efficiency is defined as the ratio between the maximum power produced by the cell and the incident power P_i of the solar radiation that arrives on the photovoltaic cell, which is normalized to 1000 W/m2 for an AM1.5 spectrum [19].

$$\eta = \frac{P_m}{P_i} = \frac{FF.V_{oc}.I_{sc}}{P_i} \quad \text{(I.2)}$$

Chapter II :
$CH_3NH_3PbI_3$
Perovskite solar cells

II.1 Introduction

PVSCs have received much attention from academia and industry owing to their low material cost, high absorption coefficient, high carrier mobility, and high conversion efficiency [20]. In 2009, a perovskite material was first introduced into solar cells, and solar cells with this kind of material exhibited a conversion efficiency of 3.9% [20]. In recent decades, great efforts have been contributed to optimize the carrier transport layers, chalcogenide layers, and interface issues to improve the conversion efficiency of PVSCs, reaching the current world record of 26.4% [20], [21].

II.2 $CH_3NH_3PbI_3$ perovskite structure

The terms ‘’perovskite’’ and’’ perovskite structure’’ are often used interchangeably. Technically, perovskite is a mineral first discovered in the Urals and named after lev perovsky (founder of the Russian Geographical Society). A perovskite structure is any compound that has the same structure as the perovskite mineral. Methylammonium lead iodide ($CH_3NH_3PbI_3$) perovskite solar cell has produced a remarkable breakthrough in the photovoltaic history of solar cell technology because of its outstanding device based performance as a light-harvesting semiconductor. The general crystal structure of perovskite is cubic.

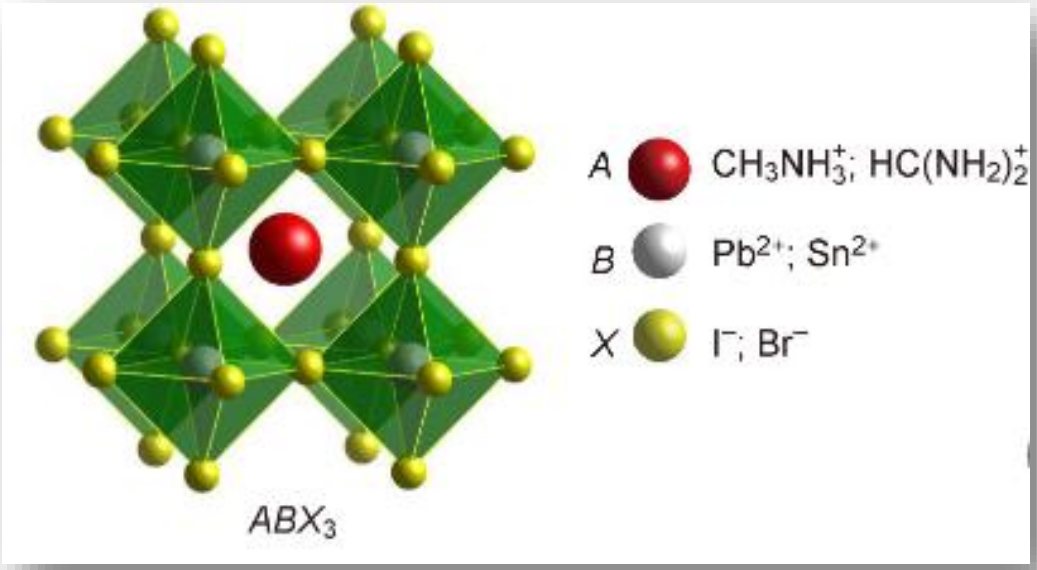

Figure II.1 : $CH_3NH_3PbI_3$ perovskite structure.

II.3 Perovskite solar cell

Halide perovskites are a family of materials that have shown potential for high performance and low production costs in solar cells. The name "perovskite" comes from the nickname for their crystal structure, although other types of non-halide perovskites (such as oxides and nitrides) are utilized in other energy technologies, such as fuel cells and catalysts. Perovskite solar cells have shown remarkable progress in recent years with rapid increases in efficiency, from reports of about 3% in 2009 to over 25% today. While perovskite solar cells have become highly efficient in a very short time, a number of challenges remain before they can become a competitive commercial technology [21].

II.3.1 General Structure of Perovskite Solar Cells

An archetypal PSC comprises an n-type compact layer, a mesoporous oxide layer, a light-harvesting perovskite layer, a hole-transporting layer and two electrodes [22]. The generic structure of a PSC is as shown in Fig II.2 and the different layers are deposited as indicated stepwise.

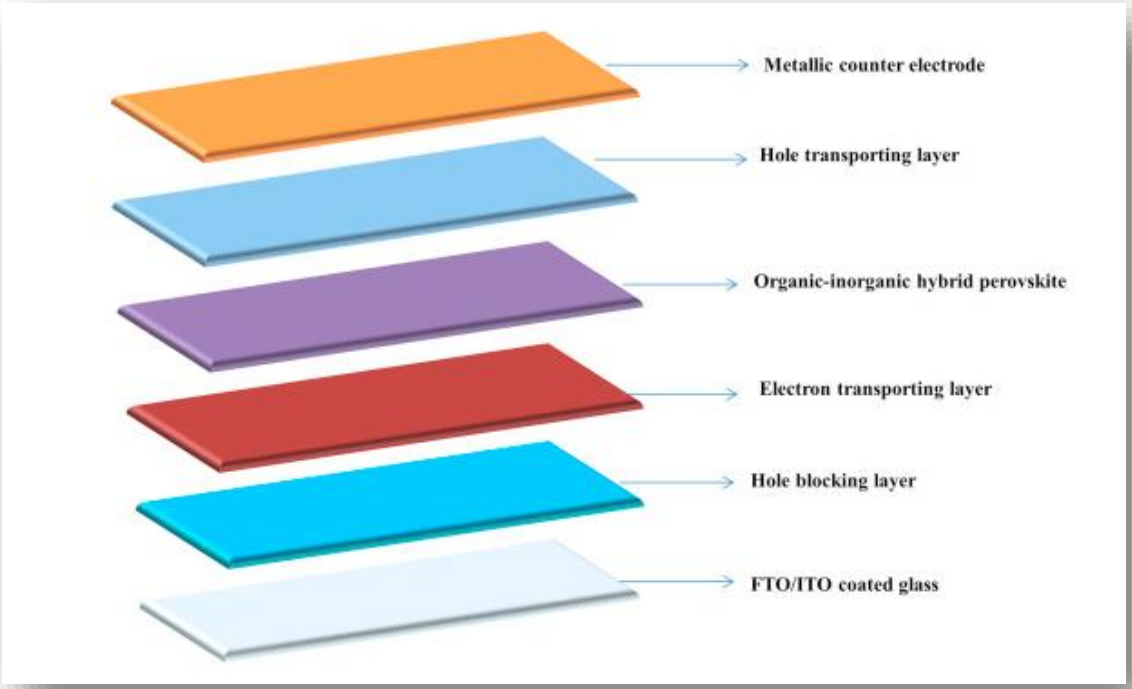

Figure II.2: Structure of Perovskite Solar Cells.

II.3.2 Operation principle of perovskite solar cell

A schematic representation of the operation principle of PSCs is illustrated in Fig II.3. Perovskite solar cells utilize perovskite structured light absorbers for photovoltaic activity like dyesensitized solar cells utilize the dye/semiconductor interface for light harvesting [23]. The photovoltaic system has three main functioning steps: (1) absorption of photons followed by free charge generation, (2) charge transport, and (3) charge extraction. When sunlight falls on a PSC, the perovskite absorbs light, excitons are generated, and charge carriers (electrons and holes) are produced upon exciton dissociation. Exciton dissociation occurs at the interface between the perovskite layer and the charge-transporting layer [23]. When the electron is separated from the hole and injected into the electron transporting layer (ETL), it migrates to the anode which is in most cases fluorine-doped tin oxide (FTO) glass. Simultaneously, the hole is injected into the hole transporting layer (HTL) and subsequently migrates to the cathode

(usually metal) [24]. The electrons and holes are collected by working and counter electrodes respectively and transported to the external circuit to produce current [25].

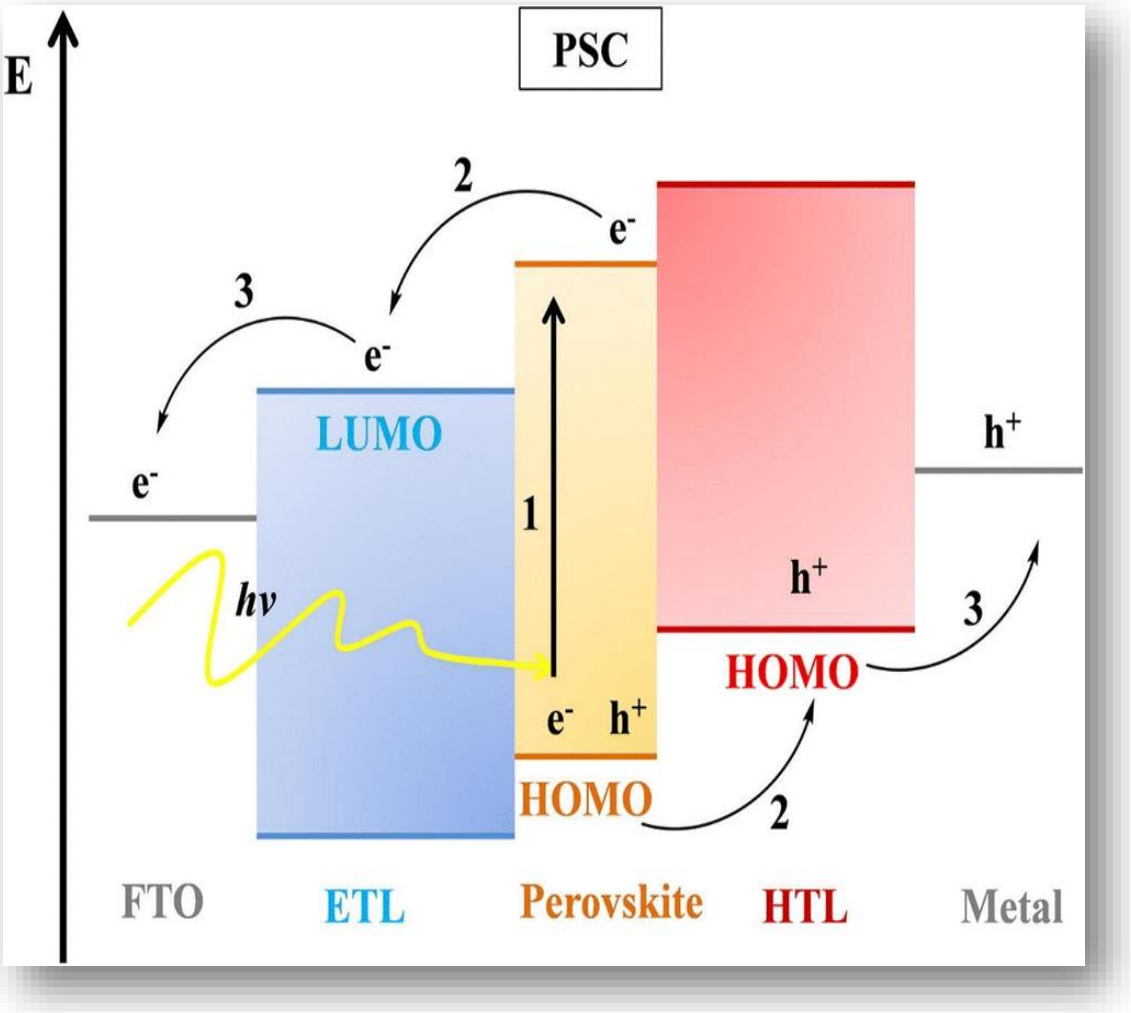

Figure II.3: Band diagram and operation principle of perovskite solar cell.

II.4 Device architecture

The device configuration is one of the most crucial factors for evaluating the overall performance of perovskite solar cells. PSCs can be classified as regular (n-i-p) and inverted (p-i-n) structures depending on which transport (electron/hole) material is present on the exterior portion of the cell/encountered by incident light first [26]. These two structures can be further

divided into two categories: mesoscopic and planar structures. The mesoscopic structure incorporates a mesoporous layer whereas the planar structure consists of all planar layers.

Perovskite solar cells without electron and hole-transporting layers have also been tested. In summary, six types of perovskite solar cell architectures have been studied by various researchers thus far: the mesoscopic n-i-p configuration, the planar n-i-p configuration, the planar p-i-n configuration, the mesoscopic p-i-n configuration, the ETL-free configuration, and the HTL-free configuration [26], [27].

The conventional n-i-p mesoscopic structure was the first arrangement of perovskite photovoltaics to be tested, in which the light-harvesting dye was replaced with lead halide perovskite semiconductors in a traditional DSSC-type architecture [28]. The interest in perovskite solar cells increased more when so-called mesoscopic device structures (Fig. II.4a) were formed by substituting the liquid electrolyte with a solid-state hole conducting material [29]. The assembly begins with a transparent glass cathode followed by the electron transportation material (ETM). The structure is then layered with a mesoporous metal oxide containing the perovskite, followed by the hole transport material (HTM), and capped with a metallic anode (Fig. II.4a). this initial advancement in PSCs created an important field of interest for photovoltaic researchers and consequently led to the development of other PSC device configurations (Fig. II.4b–d). The planar architecture is an evolution of the mesoscopic structure, where the perovskite light harvesting layer is sandwiched between the ETM and HTM. The absence of a mesoporous metal oxide layer leads to an overall simpler structure. It is possible to achieve a high efficiency without the mesoporous layer by carefully controlling the interfaces between the different layers that make up the PSC (the perovskite light absorber layer, the electron transporting layer, the hole-transporting layer, the electrodes as well as the perovskite layer itself) [29]. With the same materials and approach, a planar n-i-p PSC shows increased V_{OC} (open-circuit voltage) and J_{SC} (short-circuit current density) relative to a mesoscopic PSC device; however, the planar configuration also had more severe J-V hysteresis which calls into question the accuracy of the reported efficiencies [30]. The grain and thickness of this buffer layer influence the J-V hysteresis behavior [30], [31]. Kim et al. also observed that J-V hysteresis problem is significantly dependent on the p-type hole-transporting materials

and found that the hysteresis behavior can become negligible with a reduced capacitance, which can be done by replacing Spiro-OMeTAD with poly(3,4-ethylene dioxythiophene)-poly(styrene sulfonate) (PEDOT:PSS) or any other inorganic hole-transporting materials [32]. However, the J-V hysteresis behavior is also dependent on voltage scan direction, scan rate, and range [33]. To counter this problem, a thin mesoporous buffer layer was incorporated within the planar n-i-p PSC structure [33]. To date the best mesoscopic n-i-p device has exhibited a PCE 21.6% [34], whereas the highest reported efficiency of a planar n-i-p cell 20.7% [35]. Although mesoporous PSC shows better efficiency than planar structure, it is required to have a thinner mesoporous layer (less than 300 nm) [35]. In addition, the planar device could be fabricated with a low-temperature process unlike the mesoporous structure [36]. However, better control of the perovskite-absorbing layer is required [37].

The p-i-n PSC structured is derived from the organic solar cell [38]. In the case of the p-i-n planar perovskite architecture, the HTM layer is deposited first followed by the ETM layer. It was discovered that perovskites are capable of transporting the holes themselves [39], which led to Jeng et al. developing the first planar hetero-junction PSC with an inverted structural design [40]. With this advancement, the inverted p-i-n configuration has expanded the options to explore more for selective layer from organic to inorganic materials and the use of oxide HTM allow for constructing mesoscopic p-i-n device architecture [41], [42]. Planar p-i-n PSC offers low-temperature processing, negligible hysteresis behavior with high efficiency of 18% [41]. The device configuration of the inverted p-i-n planar and mesoscopic PSC is shown in Fig. II.4c, d.

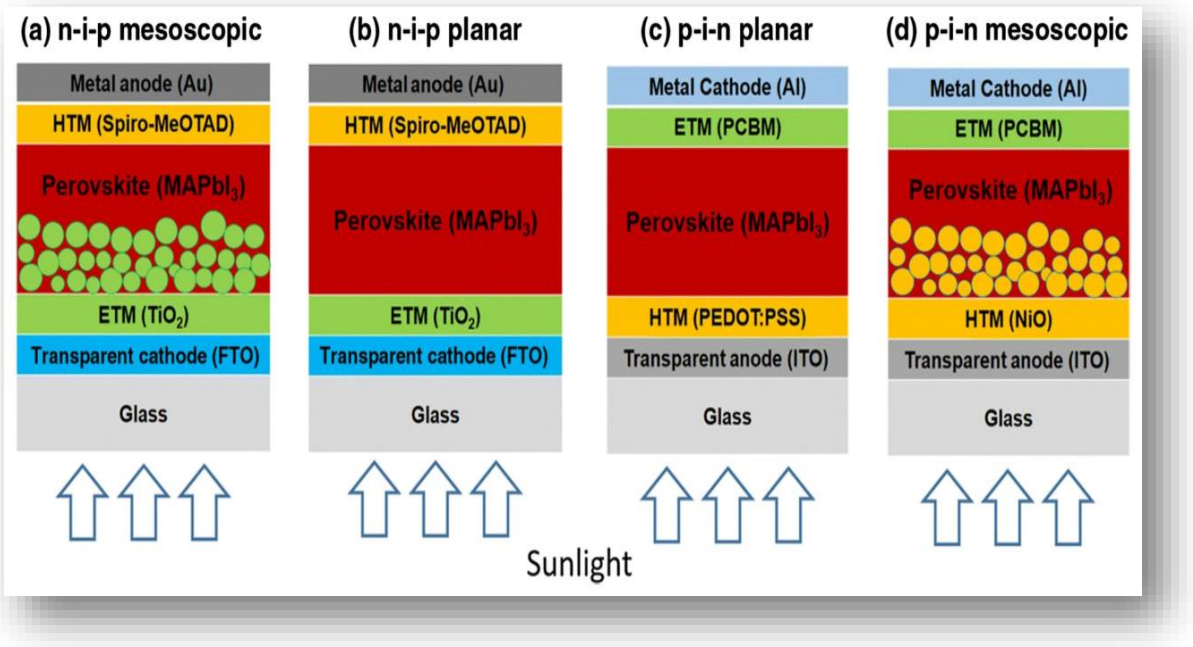

Figure II.4: Schematic showing the layered structure four typical of perovskite solar cells (a) n-i-p mesoscopic, (b) n-i-p planar, (c) p-i-n planar, and (d) p-i-n mesoscopic.

II.5 Electron-transporting layer-free structure

A compact n-type metal oxide on the transparent conductive oxide (TCO) is always required for conventional planar perovskite solar cells, as it helps to achieve high open-circuit voltage (V_{OC}) and overall power conversion efficiency. However, Hu et al. developed a surface modification technique utilizing a cesium salt solution to modify the indium– tin–oxide (ITO) surface/optimize energy level alignment at this interface, which led to a PCE of 15.1% [43]. Later, Liu et al. developed a compact layer-free PSC which exhibited 13.5% efficiency by directly depositing the perovskite layer on the ITO surface via a sequential layer deposition method, demonstrating that including an ETL is not a necessity to obtain outstanding device efficiencies [43]. Ke et al. also suggested that a TiO2 electron-transporting material may not be an ideal interfacial material after developing an efficient ETL free PSC with a PCE of 14.14% and a V_{OC} of 1.06 V grown directly on an FTO substrate via a one-step solution process without any hole-blocking layers [44]. The compact ETM layer-free planar perovskite solar cell

architecture is shown in Fig. II.5. other studies have also proved that the compact layer-free architecture can exhibit excellent performance when generated with different film-forming methodologies [45], [46].

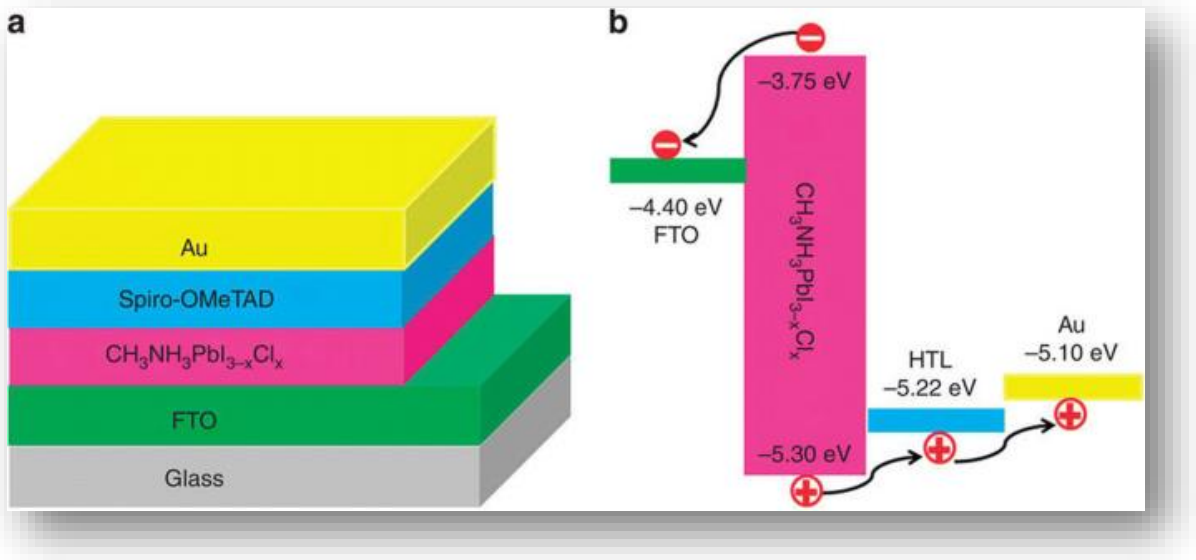

Figure II.5: (a) Schematic illustration of the electron transport layer-free planar mixed halide perovskite solar cell configuration and (b) energy level diagram of the planar PSC showing collection and separation of photo-generated electrons and holes without an ETL.

II.6 Hole transporting layer-free structure

Although various novel hole transport materials (HTMs) have been evaluated with good results (including small molecules, polymers, and inorganic compounds), HTM-free PSC architectures are a simpler cell configuration that is garnering increased attention in this field. This increasing emphasis is because most of the reported highly efficient PSCs contain expensive HTMs like fullerenes, which significantly increase the fabrication cost of the cells. As already mentioned, organo-lead halide perovskite materials show outstanding semiconducting properties like long charge transport lifetimes and an ambipolar nature which allows for the exclusion of the hole-transporting layer [47], [48]. In 2012, Etgar et al. reported the successful fabrication of HTL-free mesoscopic perovskite solar cells for the first time, indicating that MAPbI3 itself performed

the function of both a light harvester and hole conductor [49]. Aharon et al. found that the performance of HTL-free PSCs was highly dependent on the depletion layer width because this layer helps in charge separation and prevents the back-reaction of the electrons from the TiO2 with the MAPbI3 film [48]. A remarkable 12.8% certified efficiency with high stability was obtained in a fully printable hole transport layer-free mesoscopic PSC by using a double layer of mesoporous TiO2 and ZrO2 covered with porous carbon [49]. Enhancing the quality of the perovskite film and further optimization of the ETL/perovskite interface is important for further enhancement of the efficiency of HTM-free PSCs. The most straightforward hole-transporting layer-free PSC structure is shown in Fig. II.6. the different device configuration informs the selection of charge-transport (ETM and HTM) and charge-collection materials (cathode and anode). Recent advances concerning advanced materials for the electron and hole-transporting layers, as well as new materials being developed for use in the perovskite layer, are discussed in the forthcoming sections.

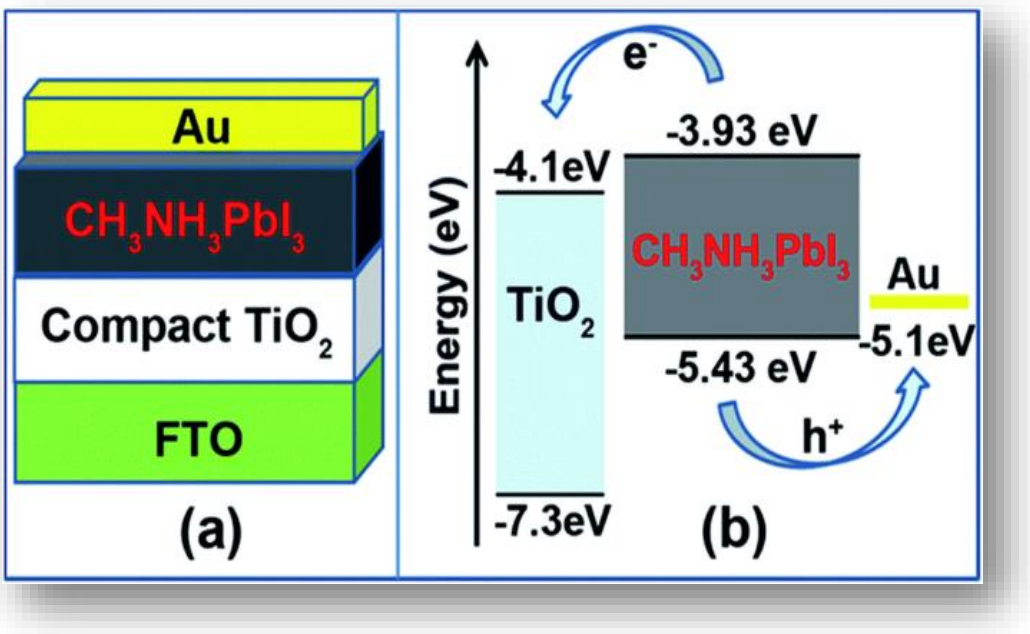

Figure II.6: Schematic illustration of the (a) structure and (b) energy level alignment of the planar hole-transporting layer-free perovskite ($CH_3NH_3PbI_3$) solar cells.

II.7 Power conversion efficiency at scale of perovskite solar cells

In small-area lab devices, perovskite PV cells have exceeded almost all thin-film technologies (except III-V technologies) in power conversion efficiency, showing rapid improvements over the past five years. However, high-efficiency devices have not necessarily been stable or possible to fabricate at large scale. For widespread deployment of perovskites, maintaining these high efficiencies while achieving stability in large-area modules will be necessary. Continued improvement in efficiency in medium-area modules could be valuable for mobile, disaster response, or operational energy markets where lightweight, high-power devices are critical.

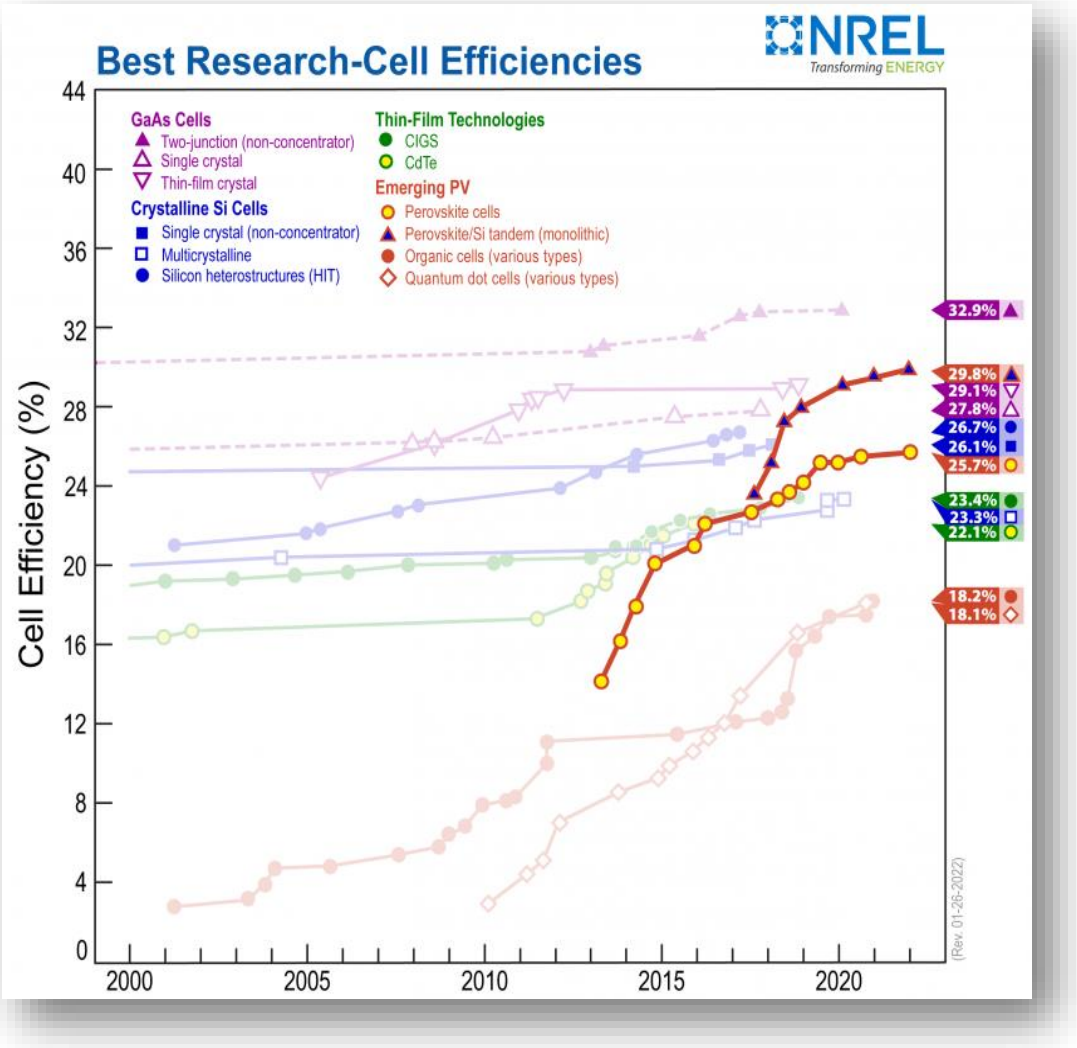

Figure II.7: Best research cells efficiencies.

Perovskites can be tuned to respond to different colors in the solar spectrum by changing the material composition, and a variety of formulations have demonstrated high performance [50]. This flexibility allows perovskites to be combined with another, differently tuned absorber material to deliver more power from the same device. This is known as a tandem device architecture. Using multiple PV materials enables tandem devices to have potential power conversion efficiencies over 33%, the theoretical limit of a single junction PV cell. Perovskite materials can be tuned to take advantage of the parts of the solar spectrum that silicon PV materials can't use very efficiently, meaning they make excellent hybrid-tandem partners [51]. It is also possible to combine two perovskite solar cells of different composition to produce a perovskite-perovskite tandem. Perovskite-perovskite tandems could be particularly competitive in the mobile, disaster response, and defense operations sectors, as they can be made into flexible, lightweight devices with high power-to-weight ratios.

II.8 Stability and durability of Perovskite Solar Cells

Perovskite solar cells have demonstrated competitive power conversion efficiencies (PCE) with potential for higher performance, but their stability is limited compared to leading photovoltaic (PV) technologies. Perovskites can decompose when they react with moisture and oxygen or when they spend extended time exposed to light, heat, or applied voltage. To increase stability, researchers are studying degradation in both the perovskite material itself and the surrounding device layers. Improved cell durability is critical for the development of commercial perovskite solar products [52].

Despite significant progress in understanding the stability and degradation of perovskite solar cells, they are not currently commercially viable because of their limited operational lifetimes. Commercial applications outside the power sector may tolerate a shorter operational life, but even these would require improvements in factors such as device stability during storage. For mainstream solar power generation, technologies that cannot operate for more than two decades are unlikely to succeed, regardless of other benefits [52].

The perovskite PV research and development (R&D) community is heavily focused on operational lifetime and is considering multiple approaches to understand and improve stability

and degradation. Efforts include improved treatments to decrease the reactivity of the perovskite surface, alternative materials and formulations for perovskite materials, alternative surrounding device layers and electrical contacts, advanced encapsulation materials, and approaches that mitigate degradation sources during fabrication and operation [53].

One issue with assessing degradation in perovskites is developing consistent testing and validation methods. Research groups report performance results based on highly varied test conditions, including different encapsulation approaches, atmospheric compositions, illumination, electrical bias, and other parameters. While such varied test conditions can provide insights and valuable data, the lack of standardization makes it challenging to directly compare results and difficult to predict field performance from test results [53].

Chapter III:
Results and discussion

III.1 Introduction

Despite the considerable efforts made to improve the efficiency of solar cells, this still remains lower than that of solar cells based on perovskite, the use of simulations for perovskite-based solar cells is becoming increasingly important to reduce design time and costs. This approach makes it possible to optimize the performance of cells, to achieve higher levels of performance. Simulation is a technique for studying real dynamical systems by simulating their behavior using a mathematical model of the system implemented on a digital computer.

Silvaco Atlas (Atlas User Manual, 2019) is one of various software incorporating this purpose and used to produce the ultrafine model based on the experimental data and analyze the behavior of optical and electrical devices under different constraints [54]. However, he must include many physical processes in order to calculate the required characteristics. In using the diffusion-drift model to model the transport of charge carriers in the device under light, wave spectrum and polarization conditions. So, it is of a two-dimensional physics simulator where all physical phenomena can be included possible such as the impact of grain size, type and density of defects, different wave spectrum as sources of illumination (irradiance), configurations and constituents of materials, as well as the fraction rate in all composite materials.

In this work, Numerical simulation is carried out using the SILVACO, for studied the performance of $CH_3NH_3PbI_3$ perovskite-based solar cells. In this study we focus on three important effects on $CH_3NH_3PbI_3$ -based perovskite solar cells, which are the thickness of the thickness of ETM region, the thickness of HTM region and the last which is the replacing of the HTM region (Spiro-OMeTAD) with PEDOT:PSS .

III.2 Features and Capabilities of ATLAS

III.2.1: Comprehensive Set of Models

ATLAS provides a comprehensive set of physical models, including [54]:

• DC, AC small-signal, and full time-dependency.

• Drift-diffusion transport models.

• Energy balance and Hydrodynamic transport models.

• Lattice heating and heatsinks.

• Graded and abrupt heterojunctions.

• Optoelectronic interactions with general ray tracing.

• Amorphous and polycrystalline materials.

• General circuit environments.

• Stimulated emission and radiation

• Fermi-Dirac and Boltzmann statistics.

• Advanced mobility models.

• Heavy doping effects.

• Full acceptor and donor trap dynamics

• Ohmic, Schottky, and insulating contacts.

• SRH, radiative, Auger, and surface recombination.

• Impact ionization (local and non-local).

• Floating gates.

• Band-to-band and Fowler-Nordheim tunneling.

• Hot carrier injection.

• Quantum transport models

• Thermionic emission currents.

III.2.2: Fully Integrated Capabilities

ATLAS works well with other software from SILVACO [54]. For example, ATLAS

• Runs in the DECKBUILD interactive run-time environment.

• Is interfaced to TONYPLOT, the interactive graphics and analysis package.

• Accepts input from the ATHENA and SSUPREM3 process simulators.

• Is interfaced to UTMOST parameter extraction and device modeling software.

• can be used in experiments with the VWF AUTOMATION TOOLS.

III.2.3: Sophisticated Numerical Implementation

ATLAS uses powerful numerical techniques, including [54]:

• Accurate and robust discretization techniques.

• Gummel, Newton, and block-Newton nonlinear iteration strategies.

• Efficient solvers, both direct and iterative, for linear sub problems.

• Powerful initial guess strategies.

• Small-signal calculation techniques that converge at all frequencies.

• Stable and accurate time integration.

III.3 Using ATLAS with Other Silvaco Software

ATLAS should only be used in conjunction with the VWF INTERACTIVE TOOLS. These include DECKBUILD, TONYPLOT, DEVEDIT, MASKVIEWS, and OPTIMIZER. DECKBUILD provides an interactive run time environment. TONYPLOT supplies scientific visualization capabilities. DEVEDIT is an interactive tool for structure and mesh specification and refinement. MASKVIEWS is an IC Layout Editor. The OPTIMIZER supports black box optimization across multiple simulators.

ATLAS is often used in conjunction with the ATHENA process simulator. ATHENA predicts the physical structures that result from processing steps. The resulting physical structures are used as input by ATLAS, which then predicts the electrical characteristics associated with specified bias conditions. The combination of ATHENA and ATLAS makes it possible to determine the impact of process parameters on device characteristics.

The electrical characteristics predicted by ATLAS can be used as input by the UTMOST device characterization and SPICE modeling software. Compact models based on simulated device characteristics can then be supplied to circuit designers for preliminary circuit design. Combining ATHENA, ATLAS, UTMOST, and SMARTSPICE makes it possible to predict the impact of process parameters on circuit characteristics [54].

ATLAS can be used as one of the simulators within the VWF AUTOMATION TOOLS. VWF makes it convenient to perform highly automated simulation-based experimentation. VWF is

used in a way that reflects experimental research and development procedures using split lots. It therefore links simulation very closely to technology development, resulting in significantly increased benefits from simulation use [54].

III.4 Physically-Based Simulation

ATLAS is a physically-based device simulator. Physically-based device simulation is not a familiar concept for all engineers. This section will briefly describe this type of simulation. Physically-based device simulators predict the electrical characteristics that are associated with specified physical structures and bias conditions [54]. This is achieved by approximating the operation of a device onto a two or three dimensional grid, consisting of a number of grid points called nodes. By applying a set of differential equations, derived from Maxwells laws, onto this grid you can simulate the transport of carriers through a structure. This means that the electrical performance of a device can now be modeled in DC, AC or transient modes of operation. There are three physically-based simulation. These are: • It is predictive. • It provides insight. • It conveniently captures and visualizes theoretical knowledge. Physically-based simulation is different from empirical modeling. The goal of empirical modeling is to obtain analytic formulae that approximate existing data with good accuracy and minimum complexity. Empirical models provide efficient approximation and interpolation. They do not provide insight, or predictive capabilities, or encapsulation of theoretical knowledge. Physically-based simulation has become very important for two reasons [54]. One, it is almost always much quicker and cheaper than performing experiments. Two, it provides information that is difficult or impossible to measure. The drawbacks of physically-based simulation are that all the relevant physics must be incorporated into a simulator, and numerical procedures must be implemented to solve the associated equations. These tasks have been taken care of for users of ATLAS. Those who use physically-based device simulation tools must specify the problem to be simulated. In ATLAS, specify device simulation problems by defining: • The physical structure to be simulated. • The physical models to be used. • The bias conditions for which electrical characteristics are to be simulated.

III.5 ATLAS Inputs and Outputs

Figure III.1 shows the types of information that flow in and out of ATLAS. Most ATLAS simulations use two input files. The first input file is a text file that contains commands for ATLAS to execute. The second input file is a structure file that defines the structure that will be simulated. ATLAS produces three types of output files [54]. The first type of output file is the run-time output, which gives you the progress and the error and warning messages as the simulation proceeds. The second type of output file is the log file, which stores all terminal voltages and currents from the device analysis. The third type of output file is the solution file, which stores 2D and 3D data relating to the values of solution variables within the device at a given bias point [54].

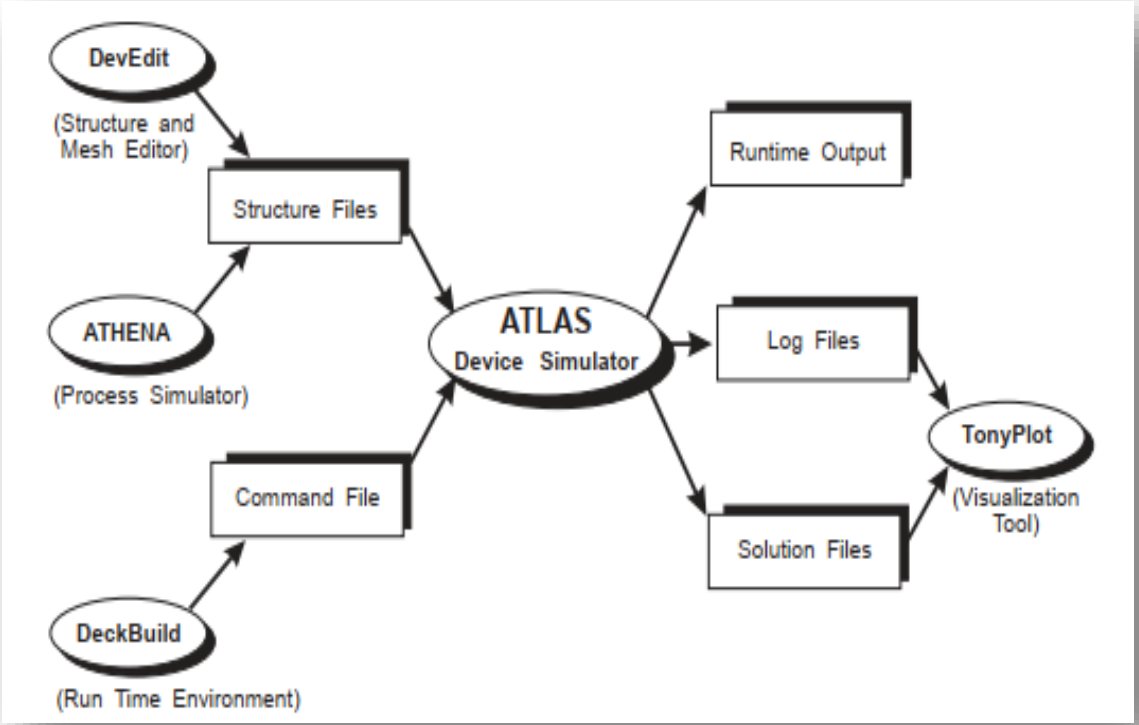

Figure III.1: ATLAS Inputs and Outputs.

III.6 ATLAS Syntax

An ATLAS command file is a list of commands for ATLAS to execute. This list is stored as an ASCII text file that can be prepared in DECKBUILD or using any text editor. Preparing an input file in DECKBUILD is preferred, which can be made easier by using the DeckBuild Commands menu in the DeckBuild Window [54].

III.6.1 Statements and Parameters

The input file contains a sequence of statements. Each statement consists of a keyword that identifies the statement and a set of parameters. The general format is:

With a few exceptions the input syntax is not case sensitive. One important exception is that commands described in this manual as being executed by DECKBUILD rather than ATLAS are case sensitive. These include: EXTRACT, SET, GO, and SYSTEM. Also, filenames for input and output under UNIX are case sensitive. For any, ATLAS may have four different types for the parameter. These are: Real, Integer, Character, and Logical. An example of a statement line is: DOPING UNIFORM N.TYPE CONCENTRATION=1.0e16 REGION=1 OUTFILE=my.dopThe statement is DOPING. All other items are parameters of the DOPING statement. UNIFORM and N.TYPE are logical parameters. Their presence on the line sets their values to true, otherwise they take their default values (usually false) [54]. CONCENTRATION is a Real parameter and takes floating point numbers as input values. REGION is an Integer parameter taking only integer numbers as input. OUTFILE is a Character parameter type taking strings as input. The statement keyword must come first but after this, the order of parameters within a statement is not important. You only need to use enough letters of any parameter to distinguish it from any other parameter on the same statement. Thus, CONCENTRATION can be shortened to CONC. REGION, but can’t be shortened to R, since there’s a parameter called RATIO associated with the DOPING statement. Logical parameters can be explicitly set to false by preceding them with the ^ symbol. Any line beginning with a # is ignored. These lines are used as comments. ATLAS can read up to 256 characters on one line. But it is best to spread long input statements over several lines to make the input file more readable. The \ character

at the end of a line indicates continuation [54].

III.7 $CH_3NH_3PbI_3$ -based perovskite solar cells structure

Over the past decade, lead halide perovskite materials have emerged as a promising candidate for third-generation solar cells and have progressed extremely rapidly. The tunable band gap, strong absorption, high power conversion efficiency, and low cost of perovskite solar cells makes them highly competitive compared to current commercialized silicon-based and thin film-based photovoltaic technologies. However, commercial products unavoidably result in large amounts of waste and end-of-life devices which can cause serious environmental impacts. To address this issue, recycle and recovery technologies of perovskite solar cells should be researched and developed proactively. In this review, the development of perovskite solar cells. The perovskite solar cell studied in this work is similar to the first n-i-p solar cell introduced by [55] but with some different. The structure of our perovskite solar cell utilized in this study is shown in (Fig III.2). It is a one-dimensional devise with n-i-p planar heterojunction. The n region is the ETL (TiO2), the i-region is the perovskite ($CH_3NH_3PbI_3$) layer and the p region is the HTL (Spiro-OMeTAD). When the cell is subject to light, excitons (bound state of an electron and a hole) are created mainly in the perovskite i layer. According to their diffusion length they can reach the n (p) region. At the n/i interface the exciton is dissociated and the electron moves toward the n layer while the remaining hole migrates towards the player. Similarly, at the i/p interface the exciton is dissociated and the hole moves to the p layer while the remaining electron migrates to the n layer. The dissociation of excitons and the migration of electrons and holes is favored by the electrical field between the n and p layers.

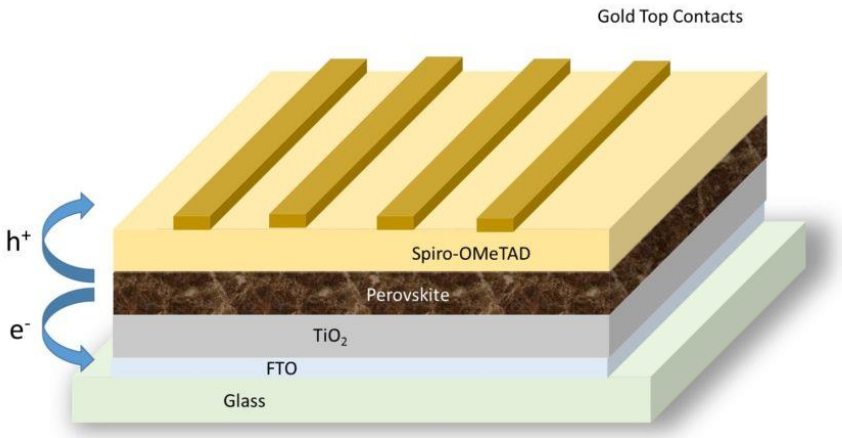

Figure III.2: Structure of $CH_3NH_3PbI_3$ -based perovskite solar cell utilized in this study.

The input parameters of the structure and the different materials are summarized in Table III.1

Table III.1: Input parameters of $CH_3NH_3PbI_3$ primary modelled perovskite solar cell.

	ETM(TiO_2)	**Perovskite**	**HTM (Spiro-OMeTAD)**
d(µm)	0.5	1.9	0.5
E_g(eV)	3.2	1.55	3.3
$\chi(eV)$	4.1	3.9	2.4
ε_r	9	6.5	9
$N_c(cm^{-3})$	2×10^{18}	2.2×10^{18}	1×10^{19}
$N_v(cm^{-3})$	1×10^{18}	1.8×10^{19}	1×10^{19}
$N_d(cm^{-3})$	2×10^{18}	5.21×10^{9}	0.0
$N_a(cm^{-3})$	1×10^{17}	5.21×10^{9}	3.17×10^{14}
$\mu_n(cm^2/Vs)$	300	40	1×10^{-3}
$\mu_p(cm^2/Vs)$	10	10	1×10^{-4}

III.8 (I-V) Characteristic of primary modelled solar cell

The current-voltage (I-V) characterization of the cell is performed to derive important parameters about the cell's performance, including its maximum current (I_{max}) and voltage (V_{max}), open circuit voltage (V_{oc}), short circuit current (I_{sc}), and its efficiency (η).The figure below shows the output characteristics of a primary modelled solar cell. This I-V curve illustrates the relationship between the current and the voltage.

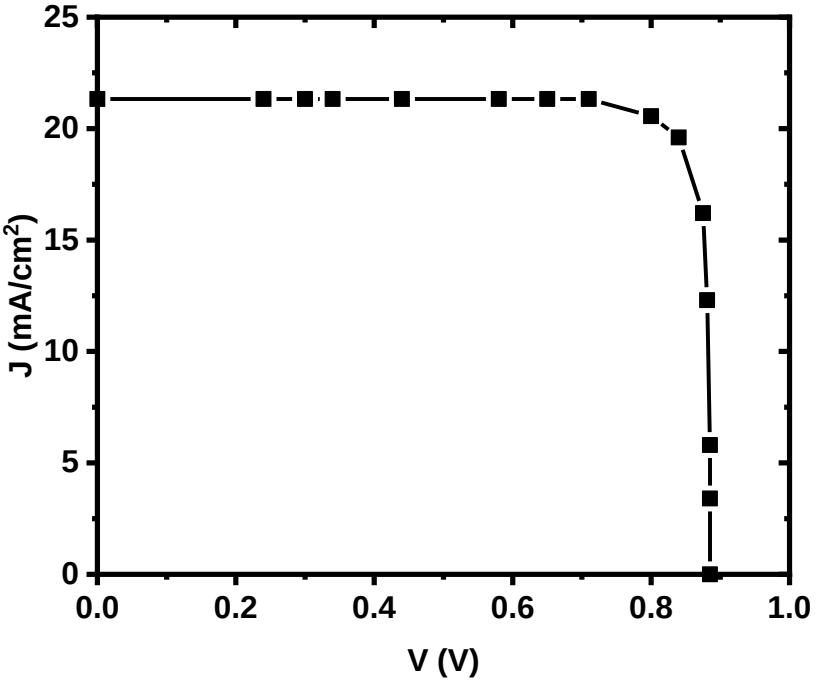

Figure III.3: (I-V) Characteristic of primary modelled solar cell.

The electrical outputs of the primary PSC solar cell are the short-circuit current density Jsc, the open-circuit voltage Voc, the fill factor FF and the conversion efficiency η are 21.33 mA/cm^2, 0.88 V, 0.72 and 14.44 %, respectively. Good agreement with experimental data was found for our results which are in the measured range of [55] and [56].

III.9 Effect of ETL (TiO_2) region thickness

The ETL in PSCs transports electrons generated from the perovskite layer [56]. It also serves as a blocking layer to hinder direct contact between the holes and FTO [57]. Hence, the layer should be pinhole free to prevent the recombination of electrons and holes at the front electrodes. Compatible energy levels support the fast injection of photogenerated electrons from perovskites and low-voltage losses. It also acts as a window layer for the perovskites; thus, a bandgap above 3 eV is necessary. The layer should electrically be as thin as possible to provide fast electron transport and low resistive losses. The titanium-oxide-based ETL is also a crucial investigation area reported in a number of studies [58], [59], [60], [61] , [62]. During the proposed solar cell simulation, all the input variables of the basic PSC are constant.

To study the effect of ETL (TiO_2) region thickness on the perovskite solar cell parameters we varied the TiO_2 region thickness from 0.5 µm to 0.1 µm.

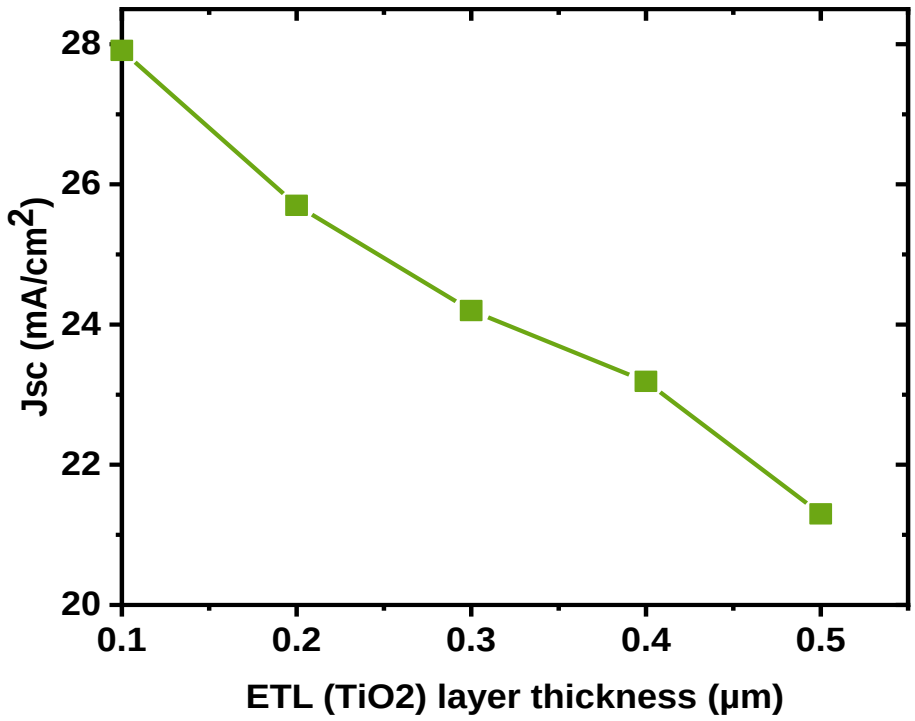

Figure III.4: Effect of ETL (TiO2) layer thickness (µm) on Jsc of the perovskite solar cell.

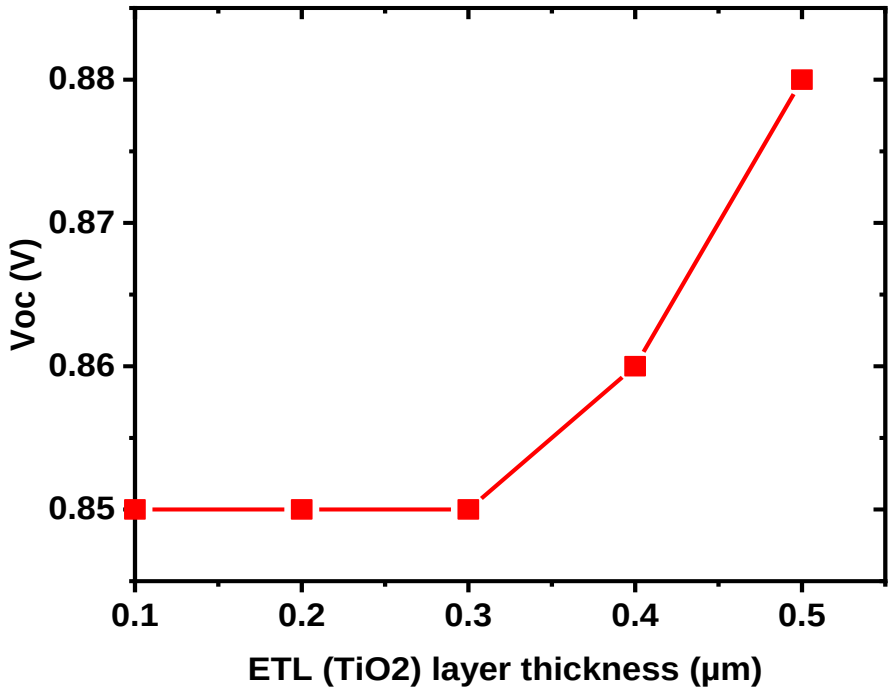

Figure III.5: Effect of ETL (TiO2) layer thickness (µm) on Voc of the perovskite solar cell.

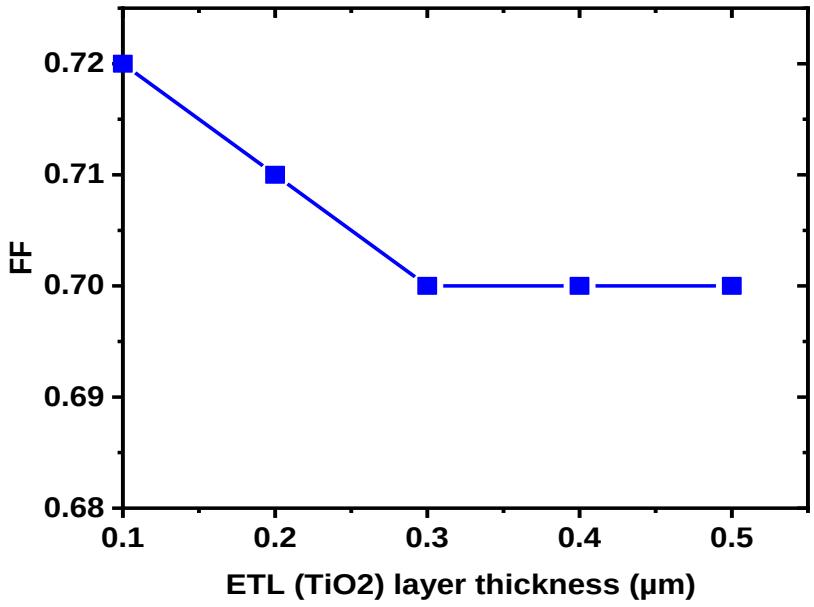

Figure III.6: Effect of ETL (TiO2) layer thickness (µm) on FF of the perovskite solar cell.

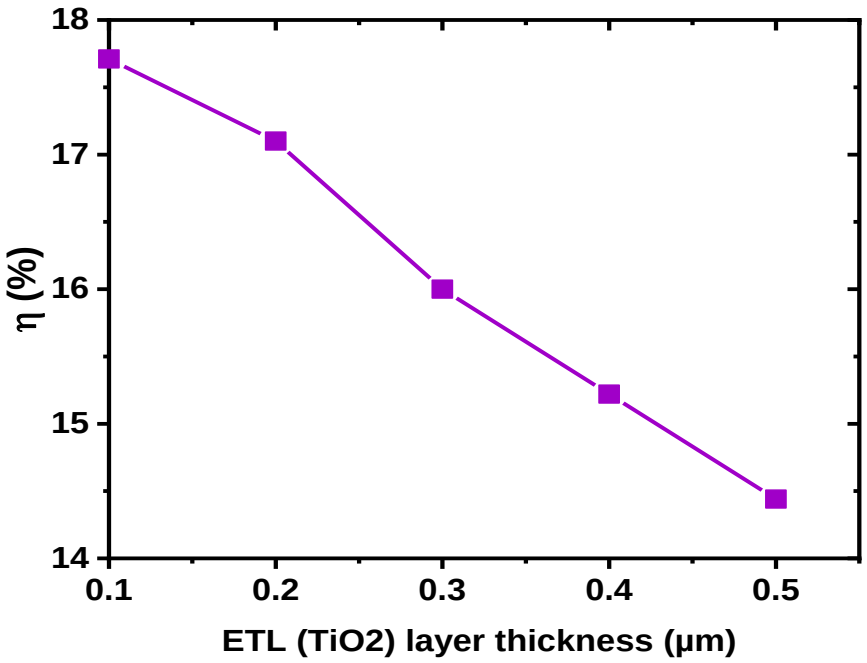

Figure III.7: Effect of ETL (TiO2) layer thickness (µm) on η of the perovskite solar cell.

The presented results clearly shows that the thickness of the compact TiO_2 ETL clearly affects the performance of $CH_3NH_3PbI_3$perovskite solar cells.

More significant effects were observed for the current density–voltage characteristics of the cells. We found that TiO_2 of thickness of 0.1 µmi s optimal, providing the best performance of the devices. Thinner layers may result in worse efficiency of cells or difficulties with the reproducibility of the devices. An ETL that is too thin may not be completely continuous and contain pinholes, which may result in fast electron–hole pair recombination at the FTO/$CH_3NH_3PbI_3$ interface. It can also provide an alternate current path for the light-generated current, lowering the Shunt resistance of the cell. It is worth noting that even the very thin layer of TiO_2 markedly increases all basic photoelectric parameters compared to the device of perovskite with thick layer of TiO_2. On the other hand, a TiO_2 layer that is too thick also has a negative impact on the performance of PSCs, as it significantly reduces the short-circuit current density (J_{SC}) and also the open-circuit voltage (V_{OC}). Along with the thickening of the TiO_2

layer from 0. 10 µmto 0.5µm, JSC decreased by 24 % (from 27.91 to 21.3 mA/cm^2) and V_{OC} (from 0.88 V to 0.85V). Yet, for most cells, the FF remained at a similar level, between 0.7 and 0.72. In effect, we noticed a clear, gradual decrease in power conversion efficiency (PCE) from 17.71 % to 14.44 % along with the thickening of the TiO_2 ETL.

III.10 Effect of HTL (Spiro-OMeTAD) region thickness

Perovskite solar cells (PSCs) are one of the most promising emerging energy-conversion technologies because of their high power conversion efficiencies (PCEs) and potentially low fabrication cost. To improve PCE, it is necessary to develop PSCs with good interfacial engineering to reduce the trap states and carrier transport barriers present at the various interfaces of the PSCs' architecture. In this subsction reports a facile method to improve the interface between the perovskite absorber layer and the hole transport layer (HTL) by minimizing the thickness of the Spiro-OMeTAD region. This method based on decreased the thickness of Spiro-OMeTAD region from 0.5 to 0.1µm.

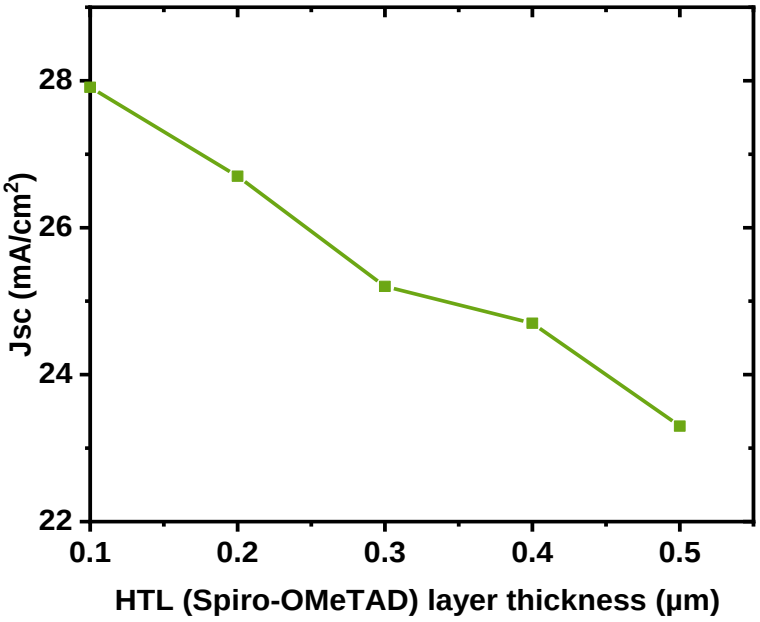

Figure III.8: Effect of HTL (Spiro-OMeTAD) layer thickness (µm) on Jsc of the perovskite solar cell.

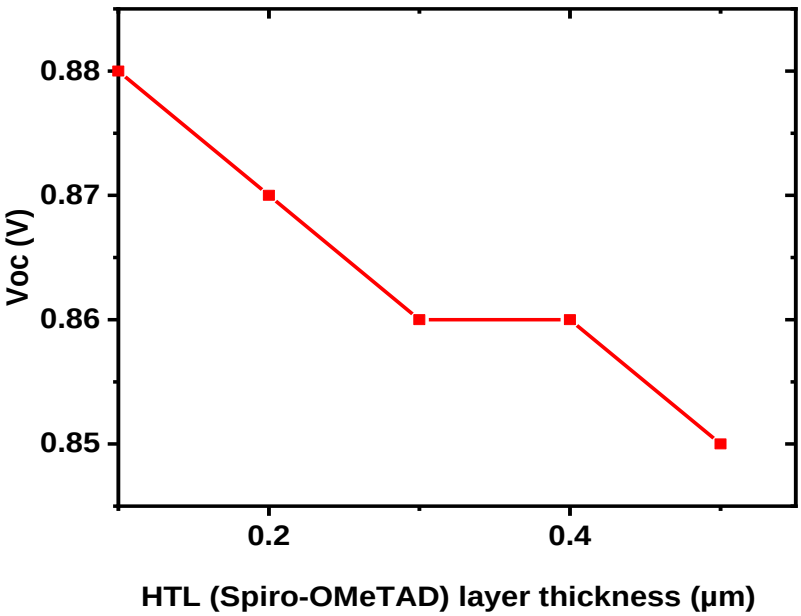

Figure III.9: Effect of HTL (Spiro-OMeTAD) layer thickness (µm) on Voc of the perovskite solar cell.

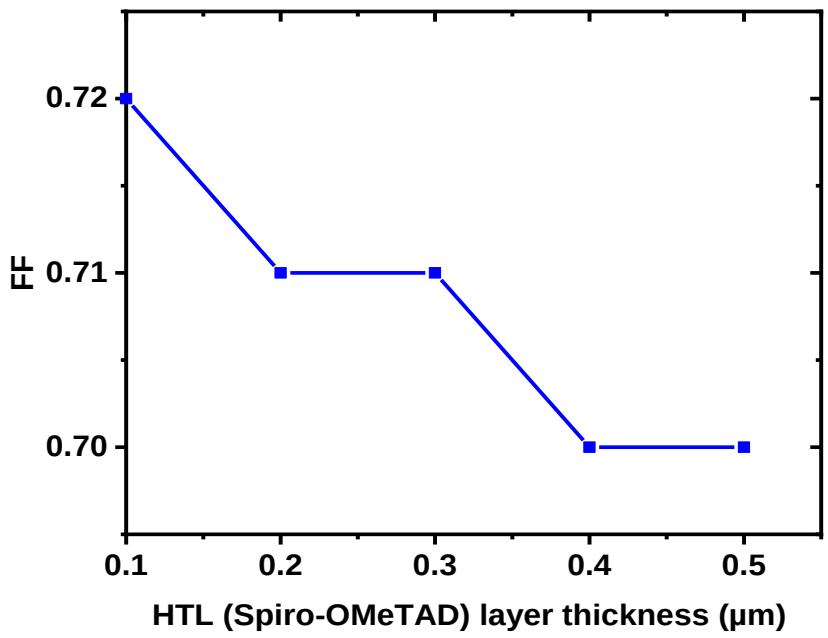

Figure III.10: Effect of HTL (Spiro-OMeTAD) layer thickness (µm) on FF of the perovskite solar cell.

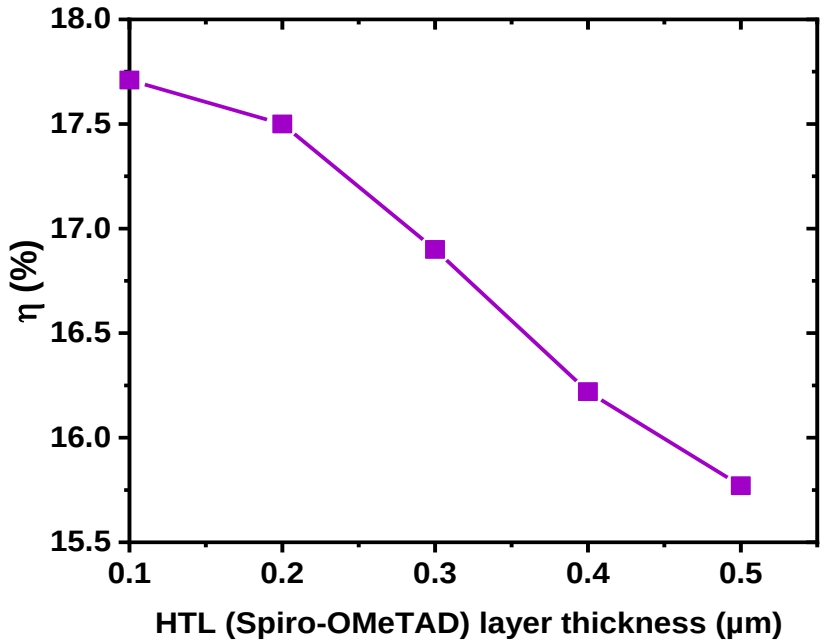

Figure III.11: Effect of HTL (Spiro-OMeTAD) layer thickness (µm) on η of the perovskite solar cell.

The result is shown that as the thickness of Spiro-OMeTAD (HTL) is decreased, the efficiency of the solar cell increases up to a certain value which is considered as optimum thickness for the solar cell. With decreasing thickness, the short circuit current (Jsc) increases the decreasing Spiro-OMeTAD(HTL) thickness allows for an improved electrical contact, enhanced collection of electrons, and reduced recombination losses at the interface between the perovskite and Spiro-OMeTAD layers and, consequently, enhances the PCE.

III.11 Effect of replacing a Spiro-OMeTAD by PEDOT: PSS material

The perovskite solar cell simulated structure is built (shown in Fig III.2) using PSCs that have been generated experimentally. In this subsection we utilized TiO_2 as ETM and changed the material of HTM were placing a Spiro-OMeTAD by PEDOT: PSS. The simulation is carried out under AMG 1.5 solar spectrum with an incident power density of 100 / mW cm2 at room temperature (300 K). Where, the input parameters of TiO_2 are extracted from [63]. The perovskites and PEDOT: PSS parameters are taken from [64], [65] and [67], respectively. The input parameters of the structure and the different materials are summarized in (Table III.2) and (Fig III.12) present the effect of replacing a Spiro-OMeTAD by PEDOT: PSS material on J-V characteristics of perovskite solar cell solar cell.

Table III.2: Input parameters of $CH_3NH_3PbI_3$ perovskite solar cell.

	ETM(TiO_2)	Perovskite	HTM (Spiro-OMeTAD)	HTM (PEDOT: PSS)
d(µm)	0.1	1.9	0.1	0.1
E_g(eV)	3.2	1.55	3.3	2.2
χ(eV)	4.1	3.9	2.45	2.9
ε_r	9	6.5	9	3
$N_c(cm^{-3})$	2×10^{18}	2.2×10^{18}	1×10^{19}	2.2×10^{15}
$N_v(cm^{-3})$	1×10^{18}	1.8×10^{19}	1×10^{19}	1.8×10^{18}
$N_d(cm^{-3})$	2×10^{18}	5.21×10^{9}	0.0	0.0
$N_a(cm^{-3})$	1×10^{17}	5.21×10^{9}	3.17×10^{14}	3.17×10^{14}
$\mu_n(cm^2/Vs)$	300	40	1×10^{-3}	
$\mu_p(cm^2/Vs)$	10	10	1×10^{-4}	

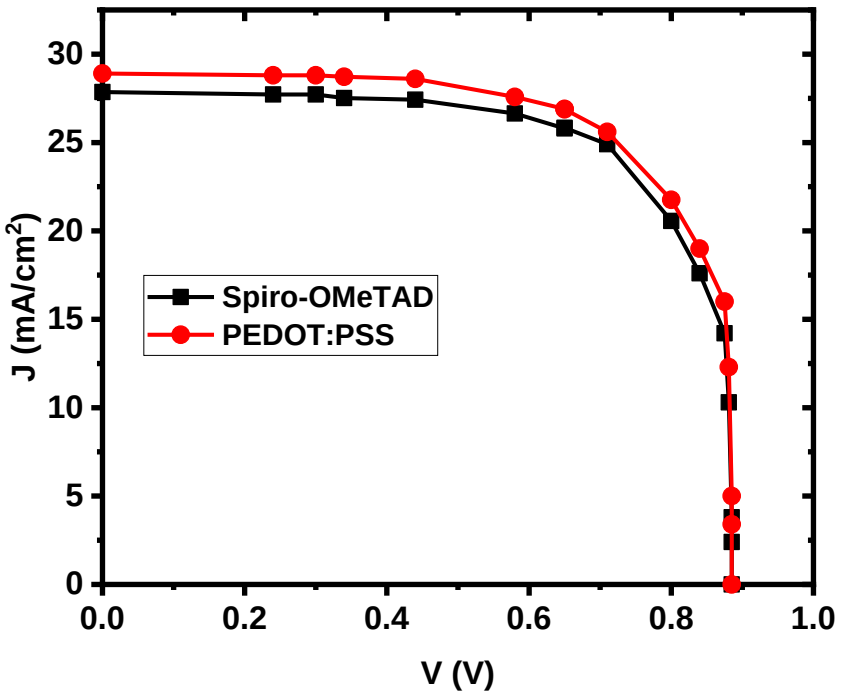

Figure III.12: Effect of replacing a Spiro-OMeTAD by PEDOT: PSS material.

As shown in Fig III.12 a slight improvement is noticed in J-V characteristics of perovskite solar cell solar cell. The PEDOT: PSS exhibited the best efficiency even if Spiro-OMeTAD exhibits the best band alignment. This is due to the holes mobility in Spiro-OMeTAD which is much smaller than holes mobility in PEDOT: PSS,when PEDOT: PSS is used as HTM in this case, the solar cell exhibits a conversion efficiency of 18.30% and a high fill factor of FF 75 %.

III.12 Conclusion

This study is an optimization of a perovskite solar cell with an n-i-p configuration using SILVACO simulator. The structure was the primary modelled solar cell which is TiO_2/Perovskite/Spiro-OMeTAD. In this chapter we have studied the perovskite solar cell performance, first, we examined the electrical characteristics (I-V) of the primary modelled solar cell, On the other hand, we focused on the thickness effect of the regions ETL and HTL effect which have the important attention in the research about the perovskite solar cells after that, we replaced Spiro-OMeTAD (HTM) with PEDOT: PSS (HTM) material and we made a comparison between them, through the obtained results we noticed that the PEDOT: PSS material improved the characteristics (I-V) of the perovskite solar cell and the optimum parameters of the thickness of ETL and HTL layers which are 0.1 µm.

General Conclusion

General Conclusion

Solar cells are typically named after the semiconducting material they are made of. These materials must have certain properties to absorb sunlight. Some cells are designed to process sunlight reaching the Earth's surface, despite the considerable efforts made to improve the efficiency of solar cells, this remains lower than that of solar cells based on perovskite, and the use of simulations for perovskite-based solar cells is becoming increasingly important to reduce design time and costs. This approach makes it possible to optimize the performance of cells, to achieve higher levels of performance. Simulation is a technique for studying real dynamical systems by simulating their behaviour using a mathematical model of the system implemented on a digital computer.

Numerical simulation is carried out using the SILVACO, to study the performance of $CH_3NH_3PbI_3$ perovskite-based solar cells. In this study, we focused on three important effects which are the thickness of ETM region, the thickness of HTM region and the last is the replacing of the HTM region (Spiro-OMeTAD) with PEDOT:PSS, the result shows that as the thickness of Spiro-OMeTAD (HTL) is decreased the performance of the solar cell increased, and also the results clearly show that the thickness of the ETL (TiO2) is more effect on the performance of $CH_3NH_3PbI_3$ perovskite solar cells than Spiro-OMeTAD (HTL). In the last the efficiency of the solar cell increased in the case of replacing Spiro-OMeTAD with PEDOT: PSS. We also made a comparison between them, and through the obtained results we noticed that the PEDOT: PSS material improved the characteristics (I-V) of the perovskite solar cell and the optimum parameters of the thickness of ETL and HTL layers which are 0.1 µm.

References

References

[1] Kojima, A.; Teshima, K.; Shirai, Y.; Miyasaka, T. Organometal Halide Perovskites as Visible-Light Sensitizers for Photovoltaic Cells. *J. Am. Chem. Soc.* **2009**, *131*, 6050–6051.

[2] O'Regan, B.; Grätzel, M. A low-cost, high-efficiency solar cell based on dye-sensitized colloidal TiO_2 films. *Nature* **1991**, *353*, 737–740.

[3] Saliba, M.; Correa-Baena, J.-P.; Wolff, C.M.; Stolterfoht, M.; Phung, N.; Albrecht, S.; Neher, D.; Abate, A. How to Make over 20% Efficient Perovskite Solar Cells in Regular (n–i–p) and Inverted (p–i–n) Architectures. *Chem. Mater.* **2018**, *30*, 4193–4201.

[4] Lee, D.G.; Kim, M.-C.; Kim, B.J.; Kim, D.H.; Lee, S.M.; Choi, M.; Lee, S.; Jung, H.S. Effect of TiO_2 particle size and layer thickness on mesoscopic perovskite solar cells. *Appl. Surf. Sci.* **2019**, *477*, 131–136.

[5] Stranks, S.D.; Eperon, G.E.; Grancini, G.; Menelaou, C.; Alcocer, M.J.P.; Leijtens, T.; Herz, L.M.; Petrozza, A.; Snaith, H.J. Electron-Hole Diffusion Lengths Exceeding 1 Micrometer in an Organometal Trihalide Perovskite Absorber. *Science* **2013**, *342*, 341–344.

[6] Jiang, Q.; Chu, Z.; Wang, P.; Yang, X.; Liu, H.; Wang, Y.; Yin, Z.; Wu, J.; Zhang, X.; You, J. Planar-Structure Perovskite Solar Cells with Efficiency beyond 21%. *Adv. Mater.* **2017**, *29*, 1703852.

[7] Zhao, Y.; Ye, Q.; Chu, Z.; Gao, F.; Zhang, X.; You, J. Recent Progress in High-efficiency Planar-structure Perovskite Solar Cells. *Energy Environ. Mater.* **2019**, *2*, 93–106.

[8] Liu, T.; Chen, K.; Hu, Q.; Zhu, R.; Gong, Q. Inverted Perovskite Solar Cells: Progresses and Perspectives. *Adv. Energy Mater.* **2016**, *6*, 1600457.

[9] Xu, L.; Chen, X.; Jin, J.; Liu, W.; Dong, B.; Bai, X.; Song, H.; Reiss, P. Inverted perovskite solar cells employing doped NiO hole transport layers: A review. *Nano Energy* **2019**, *63*, 103860.

[10] Wang, H.; Yang, F.; Xiang, Y.; Ye, S.; Peng, X.; Song, J.; Qu, J.; Wong, W.-Y. Achieving efficient inverted perovskite solar cells with excellent electron transport and stability by employing a ladder-conjugated perylenediimide dimer. *J. Mater. Chem. A* **2019**, *7*,

24191–24198.

[11] Wang, R.; Mujahid, M.; Duan, Y.; Wang, Z.-K.; Xue, J.; Yang, Y. A Review of Perovskites Solar Cell Stability. *Adv. Funct. Mater.* **2019**, *29*, 1808843.

[12] Kim, E.-B.; Akhtar, M.S.; Shin, H.-S.; Ameen, S.; Nazeeruddin, M.K. A review on two-dimensional (2D) and 2D-3D multidimensional perovskite solar cells: Perovskites structures, stability, and photovoltaic performances. *J. Photochem. Photobiol. C Photochem. Rev.* **2021**, 100405.

[13] Huang, F.; Li, M.; Siffalovic, P.; Cao, G.; Tian, J. From scalable solution fabrication of perovskite films towards commercialization of solar cells. *Energy Environ. Sci.* **2019**, *12*, 518–549.

[14] Chen, D.; Dong, H.; Pang, S.; Zhu, W.; Xi, H.; Lin, Z.; Chang, J.; Zhang, J.; Zhang, C.; Hao, Y. Enhancing material quality and device performance of perovskite solar cells via a facile regrowth way assisted by the DMF/Chlorobenzene mixed solution. *Org. Electron.* **2019**, *70*, 300–305.

[15] Du, Y.; Cai, H.; Wen, H.; Wu, Y.; Huang, L.; Ni, J.; Li, J.; Zhang, J. Novel Combination of Efficient Perovskite Solar Cells with Low Temperature Processed Compact TiO_2 Layer via Anodic Oxidation. *ACS Appl. Mater. Interfaces* **2016**, *8*, 12836–12842.

[16] Marchioro, A.; Teuscher, J.; Friedrich, D.; Kunst, M.; van de Krol, R.; Moehl, T.; Grätzel, M.; Moser, J.-E. Unravelling the mechanism of photoinduced charge transfer processes in lead iodide perovskite solar cells. *Nat. Photonics* **2014**, *8*, 250–255.

[17] Kim, T.; Lim, J.; Song, S. Recent Progress and Challenges of Electron Transport Layers in Organic–Inorganic Perovskite Solar Cells. *Energies* **2020**, *13*, 5572.

[18] Hu, W.; Yang, S.; Yang, S. Surface Modification of TiO_2 for Perovskite Solar Cells. *Trends Chem.* **2020**, *2*, 148–162.

[19] Zhou, Y.-Q.; Wu, B.-S.; Lin, G.-H.; Xing, Z.; Li, S.-H.; Deng, L.-L.; Chen, D.-C.; Yun, D.-Q.; Xie, S.-Y. Interfacing Pristine C_{60} onto TiO_2 for Viable Flexibility in Perovskite Solar Cells by a Low-Temperature All-Solution Process. *Adv. Energy Mater.* **2018**, *8*, 1800399.

[20] Huang, P.-H.; Huang, C.-W.; Kang, C.-C.; Hsu, C.-H.; Lien, S.-Y.; Wang, N.-F.; Huang,

References

C.-J. The Investigation for Coating Method of Titanium Dioxide Layer in Perovskite Solar Cells. *Crystals* **2020**, *10*, 236.

[21] Liu, D.; Li, S.; Zhang, P.; Wang, Y.; Zhang, R.; Sarvari, H.; Wang, F.; Wu, J.; Wang, Z.; Chen, Z.D. Efficient planar heterojunction perovskite solar cells with Li-doped compact TiO_2 layer. *Nano Energy* **2017**, *31*, 462–468.

[22] Chandiran, A.K.; Yella, A.; Stefik, M.; Heiniger, L.-P.; Comte, P.; Nazeeruddin, M.K.; Grätzel, M. Low-Temperature Crystalline Titanium Dioxide by Atomic Layer Deposition for Dye-Sensitized Solar Cells. *ACS Appl. Mater. Interfaces* **2013**, *5*, 3487–3493.

[23] Lee, S.-W.; Bae, S.; Cho, K.; Kim, S.; Hwang, J.-K.; Lee, W.; Lee, S.; Hyun, J.Y.; Lee, S.; Choi, S.B.; et al. Sputtering of TiO_2 for High-Efficiency Perovskite and 23.1% Perovskite/Silicon 4-Terminal Tandem Solar Cells. *ACS Appl. Energy Mater.* **2019**, *2*, 6263–6268.

[24] Möllmann, A.; Gedamu, D.; Vivo, P.; Frohnhoven, R.; Stadler, D.; Fischer, T.; Ka, I.; Steinhorst, M.; Nechache, R.; Rosei, F.; et al. Highly Compact TiO_2 Films by Spray Pyrolysis and Application in Perovskite Solar Cells. *Adv. Eng. Mater.* **2019**, *21*, 1801196.

[25] Kavan, L.; O'Regan, B.; Kay, A.; Grätzel, M. Preparation of TiO_2 (anatase) films on electrodes by anodic oxidative hydrolysis of $TiCl_3$. *J. Electroanal. Chem.* **1993**, *346*, 291–307.

[26] Starowicz, Z.; Gawlińska, K.; Walter, J.; Socha, R.P.; Kulesza-Matlak, G.; Lipiński, M. Extended investigation of sol aging effect on TiO_2 electron transporting layer and performances of perovskite solar cells. *Mater. Res. Bull.* **2018**, *99*, 136–143.

[27] Qin, J.; Zhang, Z.; Shi, W.; Liu, Y.; Gao, H.; Mao, Y. The optimum titanium precursor of fabricating TiO_2 compact layer for perovskite solar cells. *Nanoscale Res. Lett.* **2017**, *12*, 640.

[28] Wang, Y.K.; Jiang, Z.Q.; Liao, L.S. New advances in small molecule hole-transporting materials for perovskite solar cells. *Chin. Chem. Lett.* **2016**, *27*, 1293–1303.

[29] Calió, L.; Kazim, S.; Grätzel, M.; Ahmad, S. Hole-Transport Materials for Perovskite Solar Cells. *Angew. Chem.-Int. Ed.* **2016**, *55*, 14522–14545.

References

[30] Dhingra, P.; Singh, P.; Rana, P.J.S.; Garg, A.; Kar, P. Hole-Transporting Materials for Perovskite-Sensitized Solar Cells. *Energy Technol.* **2016**, *4*, 891–938.

[31] Bui, T.; Ulfa, M.; Maschietto, F.; Ottochian, A.; Nghiêm, M.; Cio, I.; Goubard, F.;Pauporté, T. Design of dendritic core carbazole-based hole transporting materials for efficient and stable hybrid perovskite solar cells. *Org. Electron.* **2018**, *60*, 22–30.

[32] Vivo, P.; Salunke, J.K.; Priimagi, A. Hole-Transporting Materials for Printable Perovskite Solar Cells. *Materials* **2017**, *10*, 1087.

[33] Jiang, X.; Yu, Z.; Zhang, Y.; Lai, J.; Li, J.; Gurzadyan, G.G.; Yang, X.; Sun, L. HighPerformance Regular Perovskite Solar Cells Employing Low-Cost Poly (ethylenedioxythiophene) as a Hole-Transporting Material. *Sci. Total Environ.* **2017**, *7*, 1–9.

[34] Mahmood, K.; Sarwar, S.; Mehran, M.T. Current status of electron transport layers in perovskite solar cells: materials and properties. *RSC Adv.* **2017**, *7*, 17044–17062.

[35] Yu, Z.; Sun, L. Inorganic Hole-Transporting Materials for Perovskite Solar Cells. *Small Methods* **2017**, *2*, 1–6.

[36] Premalal, E.V.A.; Kannangara, Y.Y.; Ratnayake, S.P.; Nalin de Silva, K.M. Facile Synthesis of Colored and Conducting CuSCN Composite Coated with CuS Nanoparticles. *Nanoscale Res. Lett.* **2017**, *12*, 1–7.

[37] Ezealigo, B.N.; Nwanya, A.C.; Simo, A.; Bucher, R.; Osuji, R.U.; Maaza, M.; Reddy, M.V.; Ezema, F.I. A study on solution deposited CuSCN thin films: Structural, electrochemical, optical properties. *Arab. J. Chem.* **2017**.

[38] Pattanasattayavong, P.; Promarak, V.; Anthopoulos, T. Electronic Properties of Copper (I)Thiocyanate (CuSCN). *Adv. Electron. Mater.* **2017**, *3*, 1–32.

[39] Ding, T.; Wang, N.; Wang, C.; Wu, X.; Liu, W.; Zhang, Q.; Fan, W.; Sun, X.W. Solution processed inorganic copper(i) thiocyanate as a hole injection layer for high-performance quantum dot-based light-emitting diodes. *RSC Adv.* **2017**, *7*, 26322–26327.

[40] Zhang, Q.; Guo, H.; Feng, Z.; Lin, L.; Zhou, J.; Lin, Z. Electrochimica Acta n-ZnO nanorods/p-CuSCN heterojunction light-emitting diodes fabricated by electrochemical method. *Electrochim. Acta* **2010**, *55*, 4889–4894.

References

[41] Petti, L.; Pattanasattayavong, P.; Lin, Y.H.; Münzenrieder, N.; Cantarella, G.; YaacobiGross, N.; Yan, F.; Tröster, G.; Anthopoulos, T.D. Solution-processed p-type copper(I) thiocyanate (CuSCN) for low-voltage flexible thin-film transistors and integrated inverter circuits. *Appl. Phys. Lett.* **2017**, *110*, 1–5.

[42] Yang, I.S.; Sohn, M.R.; Sung, S.D.; Kim, Y.J.; Yoo, Y.J.; Kim, J.; Lee, W.I. Formation of pristine CuSCN layer by spray deposition method for efficient perovskite solar cell with extended stability. *Nano Energy* **2017**, *32*, 414–421.

[43] Bakr, Z.H.; Wali, Q.; Fakharuddin, A.; Schmidt-Mende, L.; Brown, T.M.; Jose, R. Advances in hole transport materials engineering for stable and e ffi cient perovskite solar cells. *Nano Energy* **2017**, *34*, 271–305.

[44] Madhavan, V.E.; Zimmermann, I.; Roldán-Carmona, C.; Grancini, G.; Buffiere, M.; Belaidi, A.; Nazeeruddin, M.K. Copper Thiocyanate Inorganic Hole-Transporting Material for High-Efficiency Perovskite Solar Cells. *ACS Energy Lett.* **2016**, *1*, 1112–1117.

[45] Hatch, S.M.; Briscoe, J.; Dunn, S. Improved CuSCN–ZnO diode performance with spray deposited CuSCN. *Thin Solid Films* **2013**, *531*, 404–407.

[46] Xiong, Q.; Tian, H.; Zhang, J.; Han, L.; Lu, C.; Shen, B.; Zhang, Y.; Zheng, Y.; Lu, C.; Zeng, Z.; et al. CuSCN modified PEDOT:PSS to improve the efficiency of low temperature processed perovskite solar cells. *Org. Electron.* **2018**, *61*, 151–156.

[47] Chaudhary, N.; Chaudhary, R.; Kesari, J.P.; Patra, A. An eco-friendly and inexpensive solvent for solution processable CuSCN as a hole transporting layer in organic solar cells. *Opt. Mater.* **2017**, *69*, 367–371.

[48] Qin, P.; Tanaka, S.; Ito, S.; Tetreault, N.; Manabe, K.; Nishino, H.; Nazeeruddin, M.K.; Grätzel, M. Inorganic hole conductor-based lead halide perovskite solar cells with 12.4% conversion efficiency. *Nat. Commun.* **2014**, *5*, 1–6.

[49] Sepalage, G.A.; Meyer, S.; Pascoe, A.R.; Scully, A.D.; Bach, U.; Cheng, Y.B.; Spiccia, L. A facile deposition method for CuSCN: Exploring the influence of CuSCN on J-V hysteresis in planar perovskite solar cells. *Nano Energy* **2017**, *32*, 310–319.

References

[50] Qiu, L.; Ono, L.K.; Qi, Y. Advances and challenges to the commercialization of organic–inorganic halide perovskite solar cell technology. *Mater. Today Energy* **2018**, *7*, 169–189.

[51] Ramírez, D.; Riveros, G.; Álvarez, K.; González, B.; Pereyra, C.J.; Dalchiele, E.A.; Marotti, R.E.; Ariosa, D.; Martín, F.; Ramos-barrado, J.R. Electrochemical synthesis of CuSCN nanostructures, tuning the morphological and structural characteristics: From nanorods to nanostructured layers. *Mater. Sci. Semicond. Process.* **2017**, *68*, 226–237.

[52] Shlenskaya, N.N.; Tutantsev, A.S.; Belich, N.A.; Goodilin, E.A.; Grätzel, M.; Tarasov, A.B. Electrodeposition of porous CuSCN layers as hole-conducting material for perovskite solar cells. *Mendeleev Commun.* **2018**, *28*, 378–380.

[53] Murugadoss, G.; Thangamuthu, R.; Senthil Kumar, S.M. Fabrication of CH3NH3PbI3 perovskite-based solar cells: Developing various new solvents for CuSCN hole transport material. *Sol. Energy Mater. Sol. Cells* **2017**, *164*, 56–62.

[54] Device Simulator Atlas Ver. 5.10.0.R. Atlas User's Manual, SILVACO Int., Santa Clara, CA, July (2005).

[55] Wu, W.; Cui, S.; Yang, C.; Hu, G.; Wu, H. Electrochemistry Communications Electrochemically superfilling of n-type ZnO nanorod arrays with p-type CuSCN semiconductor. *Electrochem. Commun.* **2009**, *11*, 1736–1739.

[56] Chappaz-Gillot, C.; Salazar, R.; Berson, S.; Ivanova, V. Insights into CuSCN nanowire electrodeposition on flexible substrates. *Electrochim. Acta* **2013**, *110*, 375–381.

[57] Lv, Y.; Guo, Y.; Zhang, H.; Zhou, X.; Chen, H. Enhanced efficiency and stability of fully air-processed TiO2 nanorods array based perovskite solar cell using commercial available CuSCN and carbon. *Sol. Energy* **2018**, *173*, 7–16.

[58] Karuppuchamy, S.; Murugadoss, G.; Ramachandran, K.; Saxena, V.; Thangamuthu, R. Inorganic based hole transport materials for perovskite solar cells. *J. Mater. Sci. Mater. Electron.* **2018**, *29*, 8847–8853.

[59] Zhao, K.; Munir, R.; Yan, B.; Yang, Y.; Kim, T.; Amassian, A. Solution-processed inorganic copper(i) thiocyanate (CuSCN) hole transporting layers for efficient p-i-n perovskite solar cells. *J. Mater. Chem. A* **2015**, *3*, 20554–20559.

References

[60] Chowdhury, T.H.; Akhtaruzzaman, M.; Kayesh, M.E.; Kaneko, R.; Noda, T.; Lee, J.J.; Islam, A. Low temperature processed inverted planar perovskite solar cells by rGO/CuSCN hole-transport bilayer with improved stability. *Sol. Energy* **2018**, *171*, 652– 657.

[61] Wijeyasinghe, N.; Regoutz, A.; Eisner, F.; Du, T.; Tsetseris, L.; Lin, Y.H.; Faber, H.; Pattanasattayavong, P.; Li, J.; Yan, F.; et al. Copper(I) Thiocyanate (CuSCN) HoleTransport Layers Processed from Aqueous Precursor Solutions and Their Application in Thin-Film Transistors and Highly Efficient Organic and Organometal Halide Perovskite Solar Cells. *Adv. Funct. Mater.* **2017**, *27*, 1–13.

[62] Song, Z.; Phillips, A.B.; Heben, M.J.; Song, Z.; Watthage, S.C.; Phillips, A.B.; Heben, M.J.; Song, Z.; Watthage, S.C.; Phillips, A.B. Pathways toward high-performance perovskite solar cells: Review of recent advances in organo-metal halide perovskites for photovoltaic applications. *J. Photonics Energy* **2016**, *6*, 022001.

[63] Ito, S.; Tanaka, S.; Vahlman, H.; Nishino, H.; Manabe, K.; Lund, P. Carbon-Double-BondFree Printed Solar Cells from TiO2/CH3NH3PbI3/CuSCN/Au: Structural Control and Photoaging Effects. *ChemPhysChem* **2014**, *15*, 1194–1200.

[64] Yao, Y.; Wang, G.; Liao, L.; Liu, D.; Zhou, G.; Xu, C.; Yang, X.; Wu, R.; Song, Q. Enhancing the open circuit voltage of PEDOT:PSS-PC61BM based inverted planar mixed halide perovskite solar cells from 0.93 to 1.05 V by simply oxidizing PC61 BM. *Org. Electron.* **2018**, *59*, 260–265.

[65] Han, J.; Tu, Y.; Liu, Z.; Liu, X.; Ye, H.; Tang, Z.; Shi, T.; Liao, G. Efficient and stable inverted planar perovskite solar cells using dopant-free CuPc as hole transport layer. *Electrochim. Acta* **2018**, *273*, 273–281

[66] Guo, H.; Huang, X.; Pu, B.; Yang, J.; Chen, H.; Zhou, Y.; Yang, J.; Li, Y.; Wang, Z.; Niu, X. Efficiency enhancement in inverted planar perovskite solar cells by synergetic effect of sulfated graphene oxide (sGO) and PEDOT:PSS as hole transporting layer. *RSC Adv.* **2017**, *7*, 50410–50419.

[67] Castro, E.; Murillo, J.; Fernandez-delgado, O.; Echegoyen, L. Progress in fullerene-based hybrid perovskite solar cells. *J. Mater. Chem. C* **2018**, *6*, 2635–2651.

REPUBLIQUE ALGERIENNE DEMOCRATIQUE ET POPULAIRE
MINISTERE DE L'ENSEIGNEMENT SUPERIEUR
ET DE LA RECHERCHE SCIENTIFIQUE
UNIVERSITE MOHAMED KHIDER - BISKRA
Faculté des SE&SNV

الجمهورية الجزائرية الديمقراطية الشعبية
وزارة التعليم العالي والبحث العلمي
جامعة محمد خيضر بسكرة
كلية العلوم الدقيقة وعلوم الطبيعة والحياة

Département des Sciences de la matière

قسم :علوم المادة

Filière: Physique

شعبة :الفيزياء

تصريـح شرفـــي

خاص بالالتزام بقواعد النزاهة العلمية لإنجاز بحث

(ملحق القرار 1082 المؤرخ في 2021/12/27)

أنا الممضي أسفله،

السيد(ة): حمايكي جمال

الصفة: طالب سنة ثانية ماستر فيزياء تخصص: فيزياء المواد

الحامل(ة) لبطاقة التعريف الوطنية رقم: 207373818 الصادرة بتاريخ: 2022/01/16

المسجل بكلية: علوم الدقيقة وعلوم الطبيعة والحياة قسم: علوم المادة

والمكلف بإنجاز أعمال بحث : مذكرة ماستر في الفيزياء

عنوانها: study of $CH_3NH_3PbI_3$ perovskite - based solar cells performance

أصرح بشرفي أني ألتزم بمراعاة المعايير العلمية والمنهجية ومعايير الأخلاقيات المهنية والنزاهة الأكاديمية المطلوبة في انجاز البحث المذكور أعلاه وفق ما ينص عليه القرار رقم 1082 المؤرخ في 2021/12/27 المحدد للقواعد المتعلقة بالوقاية من السرقة العلمية ومكافحتها.

التاريخ: 2024/02/12

إمضاء المعني بالأمر